SKB

TECHNICAL REPORT 90-39

Modelling of the movement of the redox front in the uranium mine in Poços de Caldas, Brazil

Leonardo Romero, Luis Moreno, Ivars Neretnieks

Royal Institute of Technology, Stockholm

June 1990

SVENSK KÄRNBRÄNSLEHANTERING AB
SWEDISH NUCLEAR FUEL AND WASTE MANAGEMENT CO

BOX 5864 S-102 48 STOCKHOLM

TEL 08-665 28 00 TELEX 13108 SKB S
TELEFAX 08-661 57 19

MODELLING OF THE MOVEMENT OF THE REDOX FRONT IN THE URANIUM MINE IN POÇOS DE CALDAS, BRAZIL

Leonardo Romero, Luis Moreno, Ivars Neretnieks

Royal Institute of Technology, Stockholm

June 1990

SKB-PDC PROJECT

MODELLING OF THE MOVEMENT OF THE REDOX FRONT

Leonardo Romero
Luis Moreno
Ivars Neretnieks

Royal Institute of Technology
S-100 44 Stockholm, Sweden

June, 1990

KAT 90/24

ABSTRACT

Oxygen containing water which infiltrates reducing rock will be reduced by reaction with reducing agents in the rock. The rock will be depleted of its reducing agents and a redox front will develop. Redox sensitive elements such as uranium and some other radionuclides will precipitate in the reducing rock if they are transported into this region. This process has been suggested to take place in a repository for radioactive waste.

In an open pit uranium mine at Poços de Caldas in Brazil, the upper portions of the rock have been oxidized by infiltrating oxidizing groundwater. The redox front is very uneven and "fingering" is in evidence to depths ranging down to several hundred meters. The redox "fingers" are found in fractures and fractures zones. An attempt has been made to model the development of such redox fingerings along flow channels and to relate the structure to independent observations of flow channels in other crystalline rocks.

The rate of movement of the front has been calculated using a coupled chemical and transport model for cases which describe diffusive transport of the oxygen, advective transport of the oxygen as well flow in fractures and channels with diffusion perpendicularly from the channel walls into the rock.

TABLE OF CONTENTS

SUMMARY

The fingers of a redox front in a uranium mine at Poços de Caldas in the state of Minas Gerais in Brazil, have been modelled. The oxidation of pyrite by oxygen infiltrating with the rainwater was considered as the dominating reaction. It was assumed that this reaction is very fast and that oxygen cannot coexist with pyrite. A very sharp redox front is then formed, separating the reducing zone from the oxidized zone.

The model considers advective transport of oxidizing water and diffusion of the dissolved oxygen into the rock matrix where the oxygen reacts with the pyrite. The model accounts also for erosion and variable inlet flowrate.

Also, a set of maps (based on geochemical analytical data) provided by the geologist, were used to obtain 3-D representations of the front.

It was assumed that there are isolated channels in the rock and that different channels carry different flowrates. Having no specific data about the flow distribution and channel density, the calculations were made using the relative flowrate distribution of a Swedish site applied to the conditions at the uranium mine.

The model predicted a larger extent and faster movement of the front than what was observed in the mine.

1 INTRODUCTION

Natural analogue studies of migration of radionuclides through geological sites, have been accepted as a means to provide useful information on processes and mechanisms considered to be significant to the radioactive waste disposal concepts. One of these analogues is an open pit Uranium mine, which has been operated by the Nuclebras Company at Poços de Caldas, PDC, in the state of Minas Gerais in Brazil, since 1975. The international Poços de Caldas project is a study of many processes including redox front movement, matrix diffusion, colloids and microorganisms as well as radionuclide migration.

In the C-09 Osamu Utsumi uranium mine, the redox front is estimated to have formed and moved during many millions of years, although the exact age of the rock formation and the rate of the weathering process is uncertain. Estimates ranging between 70-90 million years have been made.

This study of the movement of the redox front considers the oxidation of pyrite as the principal reaction. It includes the transport mechanisms of advective flow, diffusion into and chemical reaction within the rock matrix. Of special interest is also the formation of large scale "fingering" of the redox front along paths of higher hydraulic conductivity. The present day redox front has evolved over long times and erosion must probably be accounted for in the modelling of the formation and movement of the front. The topography, hydraulic properties of the rock, and rates of infiltration of water have certainly changed over time so that the present day shape and location of the front is the result of processes which have varied over time.

The aims of this report is to study if the movement of the redox front may be explained by the water infiltration through of fractures. The effect of the erosion is also included as well as the stochastic nature of the flow processes involved.

2 DESCRIPTION OF THE MINE

The open pit mine lies along a valley bottom. It is several hundreds meters wide, nearly 1 km long and more than hundred meters deep in some places. The mine has near vertical terraced walls where the rock is accessible and visible. The bedrock is crystalline and consists mainly of phonolites and nepheline-syenites. The deeper portions of rock contain about 2 % by weight of pyrite (FeS_2) and are strongly reducing. However, the upper portions have became oxidized by infiltration of rainwater. The hydraulic conductivity is around 10^{-6} m/s [Smellie et al., 1987], with a trend to decrease with depth. The bedrock porosity ranges around 4-20 %. The higher porosity is found in the oxidized region and the lower in the reduced region. Water samples taken from boreholes in the reducing rock, show a characteristic reducing groundwater of low pH, around 5-6 with values of Eh-measurements ranging around -450 mV and relatively low ionic strength [Smellie et al., 1987].

Taking into consideration the chemistry of the Poços de Caldas nepheline-syenites which suggests a degree of crystallization under certain pressure conditions and the coexistence of fine-grained phonolites with rock of larger grain size (nepheline-syenites), the erosion of the rock over the last 90 million years has been estimated to be 3-9 km depth [Ulbrich, 1989]. Observations of dissolved solids and suspended matter in local rivers, indicate a maximum erosion and dissolution of about 12 km during the same period [Lei, 1984].

The redox front movement and the deposition of uranium are clearly seen on the walls of the mine and in the boreholes from the floor. Uraninite nodules are found in many places just below the redox front in the reduced rock. Figure 2-1 shows a cross-section of the rock below the present day mine level. There is a very sharp redox front delineating the upper oxidized rock from the deeper reduced rock. The reducing zone is rich in pyrite and the oxidized zone is practically devoid of pyrite. There are also many fingers of oxidized rock extending much further downward than the average depth of the front. The fingering is often associated with fractures and these fractures are sloping at various angles so that the fingers are often not vertical but at some low angle.

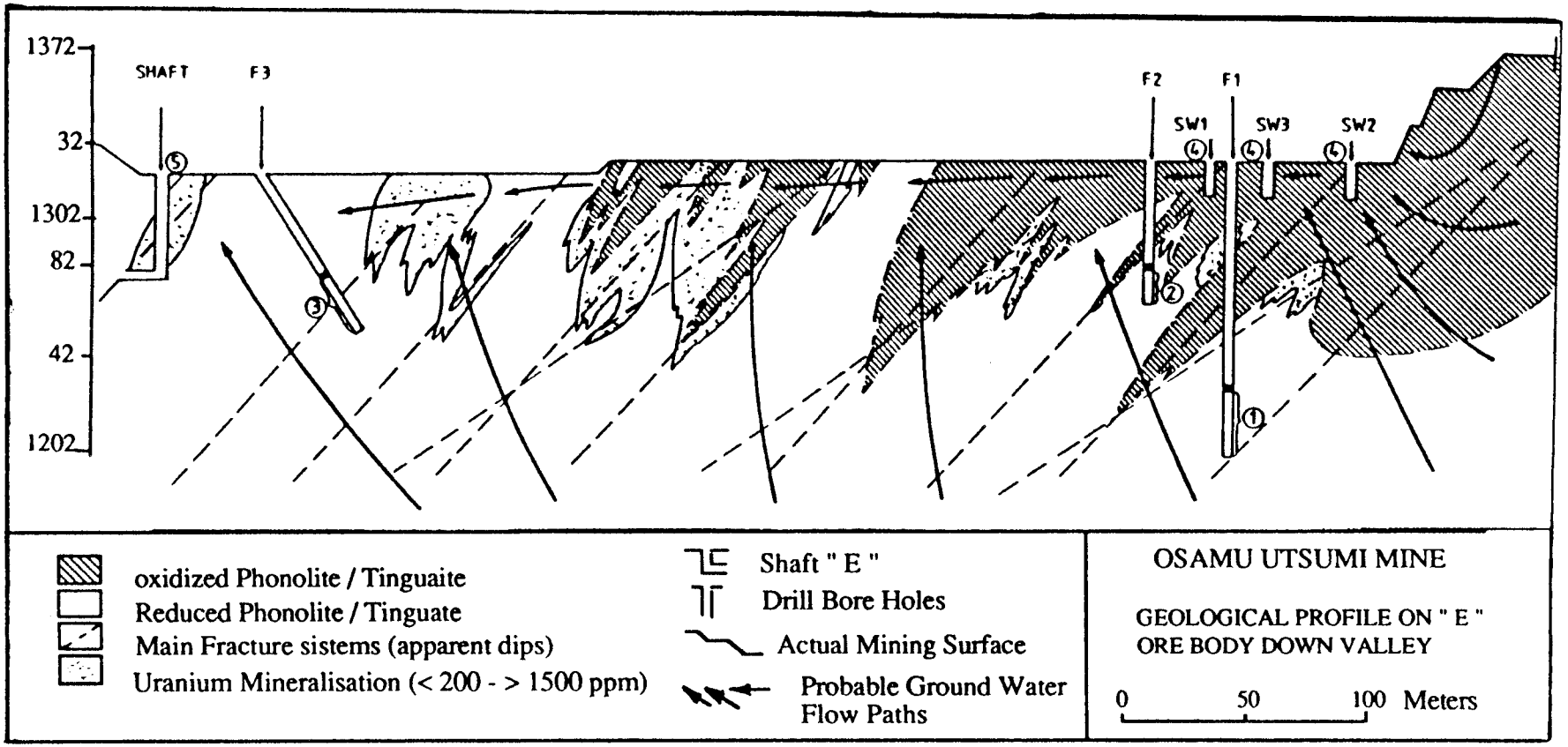

Figure 2-1 A cross-section of the uranium mine showing the redox front "fingers".

2.1 OXIDATION OF THE PYRITE

The oxidation of pyrite is a complex process [Zhu, 1988] because it involves competing redox reactions of at least two ion pairs Fe^{2+} / Fe^{3+} and S^{-} / S^{6+}. It has been reported that the oxidation by oxygen is dominant. The Fe^{2+} is released from the pyrite, either by dissolution or by oxidation of sulfur. The reaction is also catalyzed by microbial processes. Several reaction paths are possible.

$$FeS_2\ (s) \ ===> \ Fe^{2+} + S_2^{2-} \qquad (2.1)$$

$$FeS_2\ (s) + 8H_2O \ ==> \ Fe^{2+} + 2SO_4^{2-} + 16H^{+} + 14e^{-} \qquad (2.2)$$

S_2^{-2} is possibly a very unstable intermediate product which will be immediately oxidized once it is formed. The release of sulfur from the pyrite is likely to be accompanied by immediate oxidation reactions. The dissolved Fe^{2+} is oxidized by the dissolved oxygen.

$$O_2\ (aq) + 4H^{+} + 4e^{-} \ ===> \ 2H_2O \qquad (2.3)$$

$$Fe^{2+} \ ===> \ Fe^{3+} \ + e^{-} \qquad (2.4)$$

Under appropriate pH conditions, the Fe^{3+} may be precipitated first in an amorphous structure and then later converted to a stable crystalline form, ferric hydroxide. This can be transformed to form hematite (Fe_2O_3) or geothite (FeO(OH)). A mix of ferrous and ferric oxide, magnetite (Fe_3O_4 --> $FeO.Fe_2O_3$) is also one of the solid phases commonly observed. The relative stability of the ferric precipitates is not clear either, thus in this model, only $Fe(OH)_3$ is considered. The assumption of this end product does not influence the results of the calculations because the mass balance is the same and reaction rates are assumed to be so fast that equilibrium is always maintained. The groundwater in the rock is acidified considerably by the protons produced by the pyrite oxidation reaction and this is thought to be the major cause of the acid drainage in the mine.

The overall net reaction is

$$FeS_2\,(s) + \frac{15}{4}O_2\,(aq) + \frac{7}{2}H_2O \Rightarrow Fe(OH)_3\,(s) + 4\,H^{+} + 2\,SO_4^{2-} \qquad (2.5)$$

3 REPRESENTATION OF THE REDOX FRONT IN 3-D FROM MINE MAPS

In the uranium mine (Osamu Utsumi), the deeper parts of the bedrock are strongly reducing while the upper parts have became oxidized by oxygen carried by infiltrating rainwater. The redox front is very sharp. In locations with high permeability (i.e. fractures or fracture zones) "fingers" of oxidized rock are extending much further downward into the bedrock than the average depth of the front.

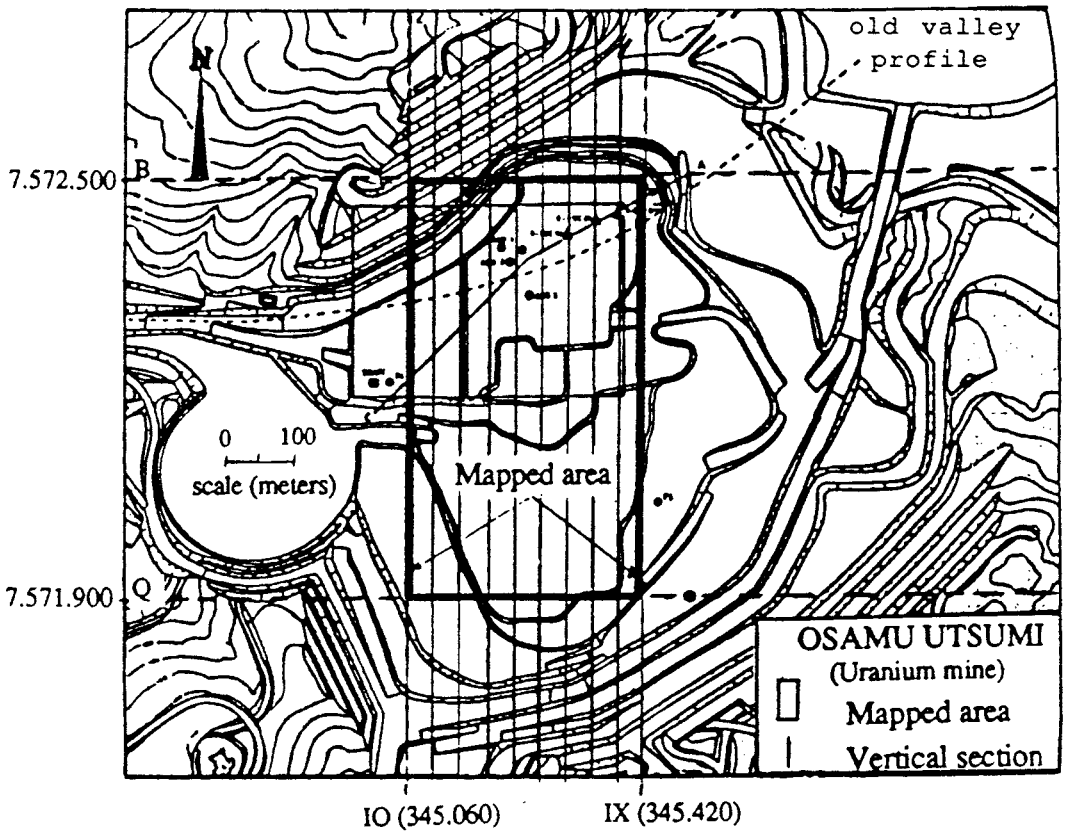

Figure 3-1. Location of the mapped area studied. The vertical lines show the location of the vertical sections used.

3.1 LOCATION OF STUDY ZONE

The mine has been divided in three large zones and mapped in great detail during the excavation. A set of 10 maps provided by the mine geologists have been used to obtain the 3-D representation of the front. These maps, which have been based on geochemical analytical data, show the location of the redox front for any given vertical section. The zone covered in this study is about 216.000 m^2 (600 by 360 m). The profiles are located in the S-N direction covering a distance of more than 600 m, and spaced every 40 m in W-E direction over a distance of 360 m. Figure 3-1 shows the study zone and the location of the profiles used.

The redox front which is located between 1200 - 1400 meters above sea level, is influenced by deeply penetrating conductive fractures which are sloping at various angles into the bedrock. The redox front is not always moving vertically downwards. To simplify computations, the location of the redox front has been slightly modified to get only one vertical location. Figure 3-2 shows the location of the redox front for a given section and the modified profile used to represent the 3-D diagrams.

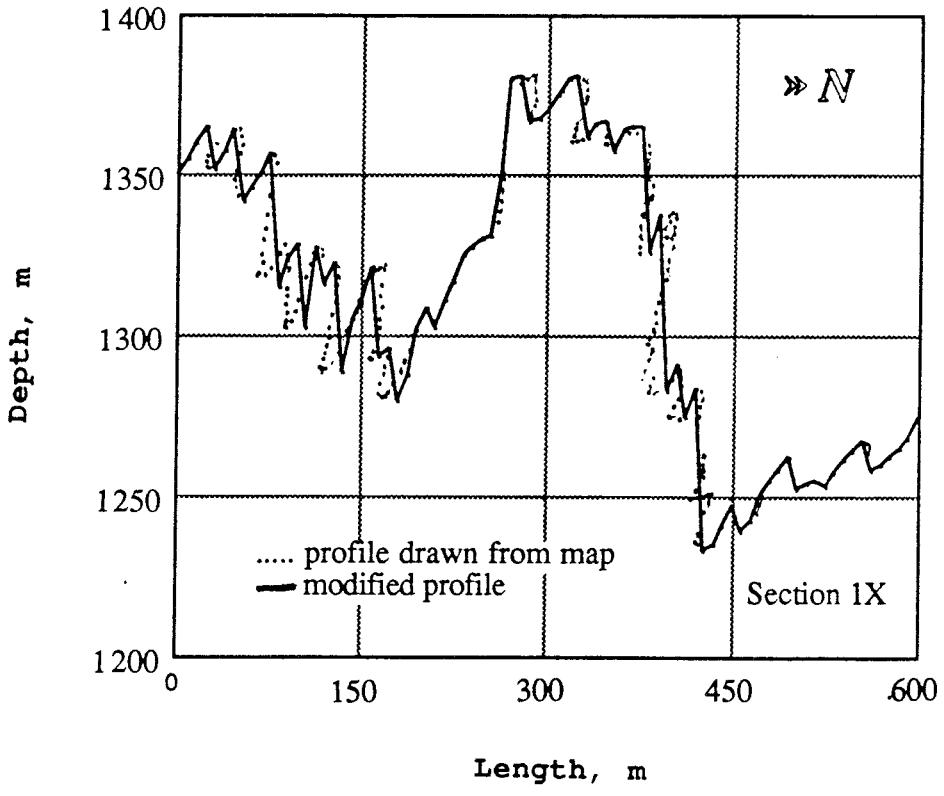

Figure 3-2. Location of the redox front for a given section and the modified profile.

3.2 THE 3-D PLOTS

From the data a 3-D computer model has been devised showing the location of the redox front. The Figures 3-3 a,b,c, and d illustrate the 3-D location of the redox-fingers from different view points through the mine, in an area of 600x360 m. The diagrams clearly show the existence of several downward penetrating "fingers" of oxidized bedrock, along and adjacent to fractures or fracture zones of greater permeability than the rock matrix itself. Because of the variability of the hydraulic properties within these zones, the "fingers" are not uniformly distributed.

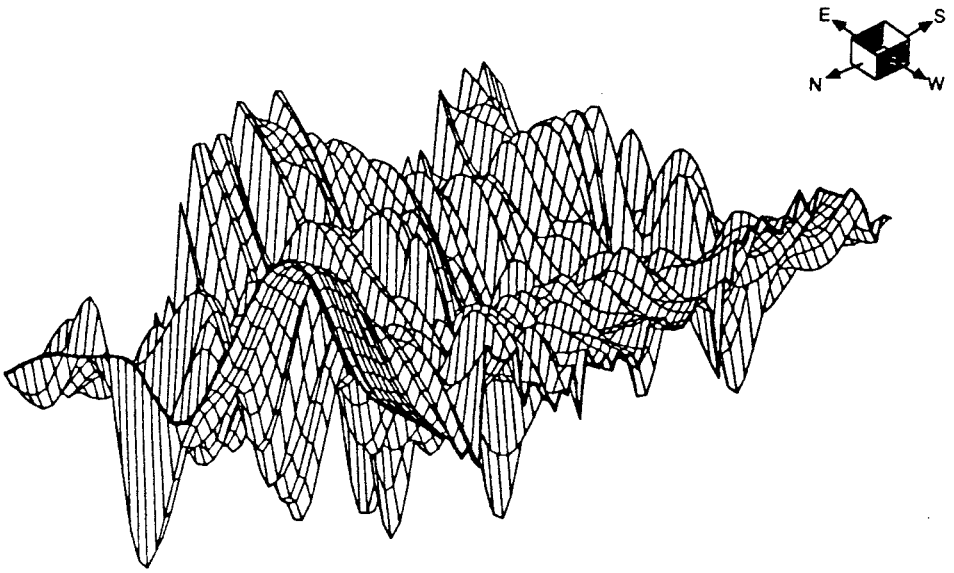

Figure 3-3a A 3-D view of "fingers". Slanting view from above. The box shows the orientation.

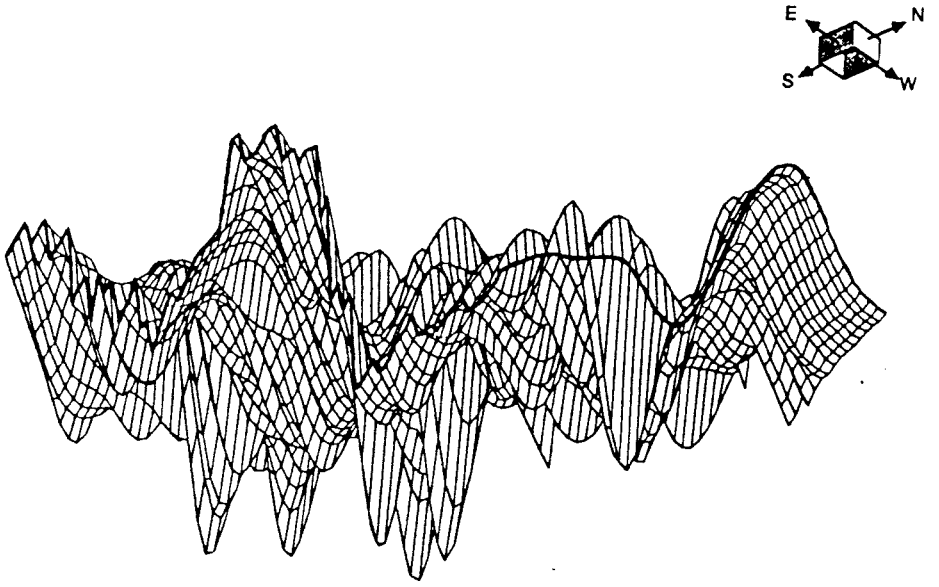

Figure 3-3b A 3-D view of "fingers". Slanting view from below. The box shows the orientation.

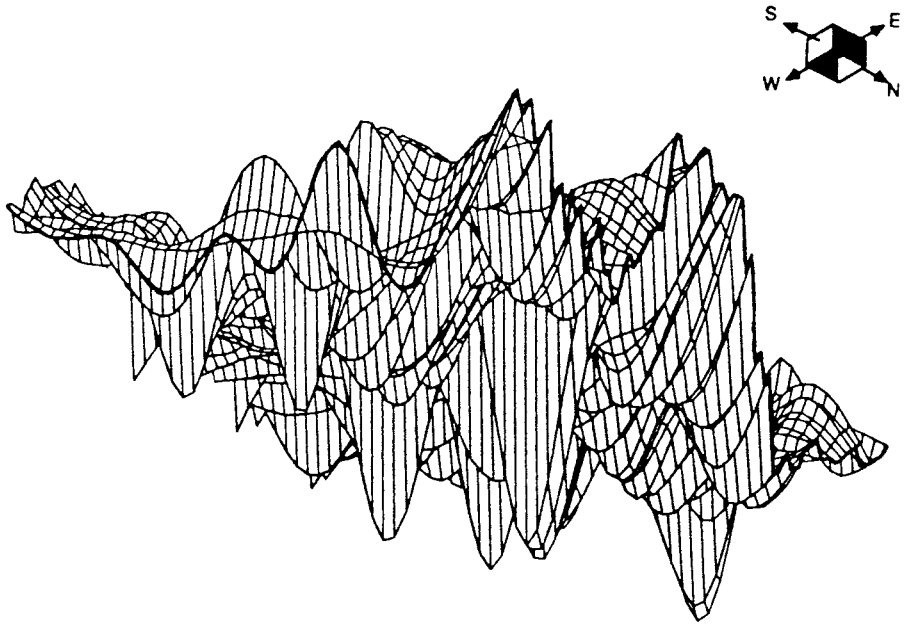

Figure 3-3c A 3-D view of "fingers". Slanting view from below. The box shows the orientation.

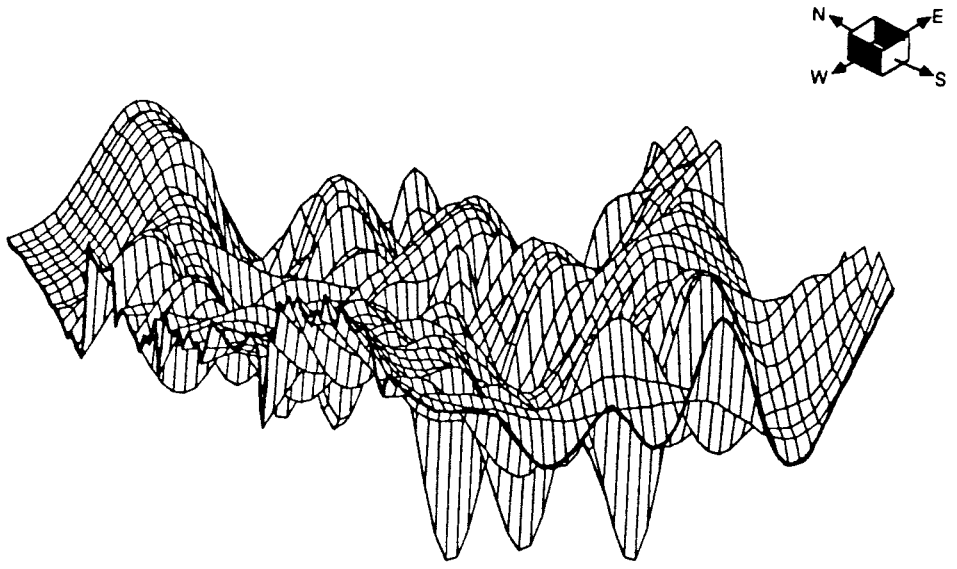

Figure 3-3d A 3-D view of "fingers". Slanting view from above. The box shows the orientation.

The depths of the fingers are shown in Figure 3-4, and the total number of redox fingers defined in the area is 134 over the studied area of 216 000 m^2. The reference level is 1200 m over the sea level.The frequency of redox fingers is on the order of 1/1000 m^2. The fingers in the mined away rock could not be reconstructed. The number of channels is thus truncated and gives too few channels. The resolution of the mapping is very coarse (in a grid of 40x40 m a maximum of 64 boreholes are made but in practice not all were driven and in some places none of them) and finer channels than those that can be picked up in a 5x5 m box will not be found. Visual observations in the vertical walls show many fine channels but these have not been quantified in the histogram.

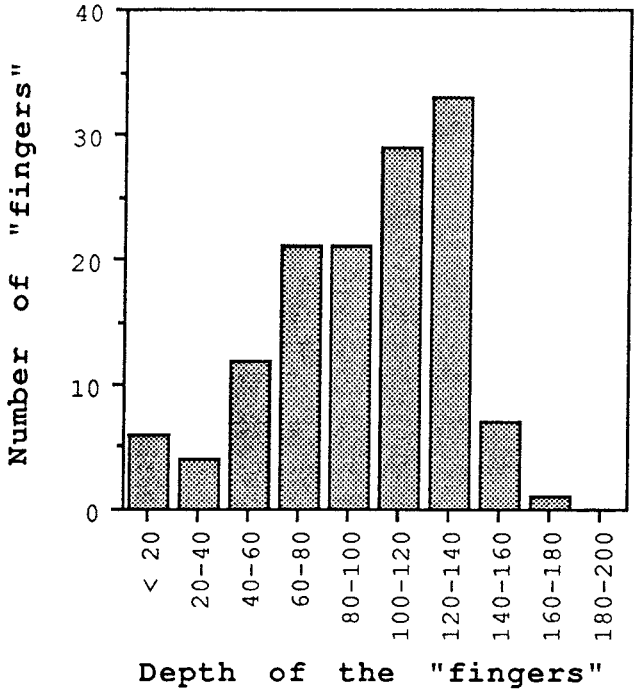

Figure 3-4 Distribution of the depth of the redox-fingers in the site. The scaling of the depth takes as reference 1200 meters over the sea level.

4 SIMULATION OF THE REDOX FRONT MOVEMENT USING A CHANNELING MODELLING

Zhu (1988), tested different approaches in an effort to model the redox front movement. He considered the diffusion and/or flow in a porous medium and also in a fractured medium. The oxidation reaction of pyrite was considered to be the dominating reaction. Oxygen was assumed to intrude with infiltrating groundwater.

He found that oxygen from the surface could not penetrate far by diffusion only. Advective flow in porous rock could carry the dissolved oxygen to larger depths. Assuming that 100 mm rainfall per year infiltrates it would take about 1 million year for the front to reach a depth of 25 m. This rate of movement is of the same magnitude as the estimated rate of erosion and suggests that there may be a stationary situation with the redox front keeping just ahead of the erosion.

A case with flow in fractures and diffusion of oxygen into the porous rock matrix from the water flowing in the fracture was also considered. The results obtained for a dense fracture spacing of 1 m and an average flowrate equivalent to 100 mm infiltrating rainwater showed that the peaks of the redox front take a time of 1-3 million years to reach a length of 40-70 m along the fractures. With larger fracture spacings, where more water must flow in every fracture, the tips of the redox front in the fractures can move very much faster. It was found that the spacing of conductive fractures and thus the water flowrate per fracture was one of the most important entities which determine the depth of redox front in the fractures.

4.1 CONCEPTUAL MODEL

In the present model we assume that there are isolated channels in the rock and that different channels carry different flowrates.

A part of the rainwater infiltrates into the rock. The water is saturated with oxygen and has a concentration of approximately 10 ppm. The rock contains pyrite which is the main reducing component. Some of the water flows into the porous rock matrix directly but some of the water flows into channels, fractures, and fracture zones with higher permeability than the rock matrix. In the fractures and fracture zones there are regions of higher permeability which results in preferential flow along these paths. We call them channels.

Figure 2-1 shows that redox "fingers" have formed and we relate these "fingers" to the channels with the higher flowrates. The water infiltration occurs through sparse channels in the rock. It is assumed that these channels are randomly distributed, have a given frequency and different flowrates.

The oxygen in the infiltrating water is transported by diffusion from the water in the channel to the location where the pyrite still is unreacted. Here the oxygen is consumed by reaction with the pyrite. The reaction is very fast compared with the velocity of oxygen transported by diffusion. The oxidation of pyrite by oxygen, Equation (2.5), is considered to be the dominating reaction.

The redox front is at the position where the pyrite has been consumed. For simplicity the reaction is considered instantaneous and irreversible which results in a sharp redox front which separates the oxidized zone from the reducing rock.

The rock is modelled as a fractured porous medium containing sparse channels in the fracture planes. At early times, the advance lines of the redox front perpendicular to the channel into the matrix may be represented by a linear model. The oxidized zone is nearly rectangular initially, but with time this zone becomes oval and finally circular. This is shown in Figure 4-1, for a horizontal cross-section of the rock. For modelling purposes we assume that propagation of the front is cylindrical already from the start.

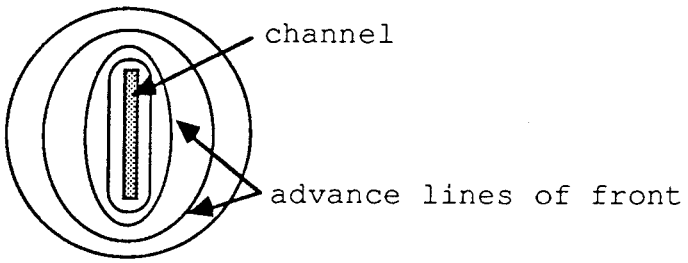

Figure 4-1 Redox front develops outward from channel by diffusion. With time, the redox front expands outward. View from above.

Figure 4-2 shows the development of the reducing finger along a fracture or channel seen from the side and Figure 4-3 shows a fracture that is expanded to obtain a cylindric annulus.

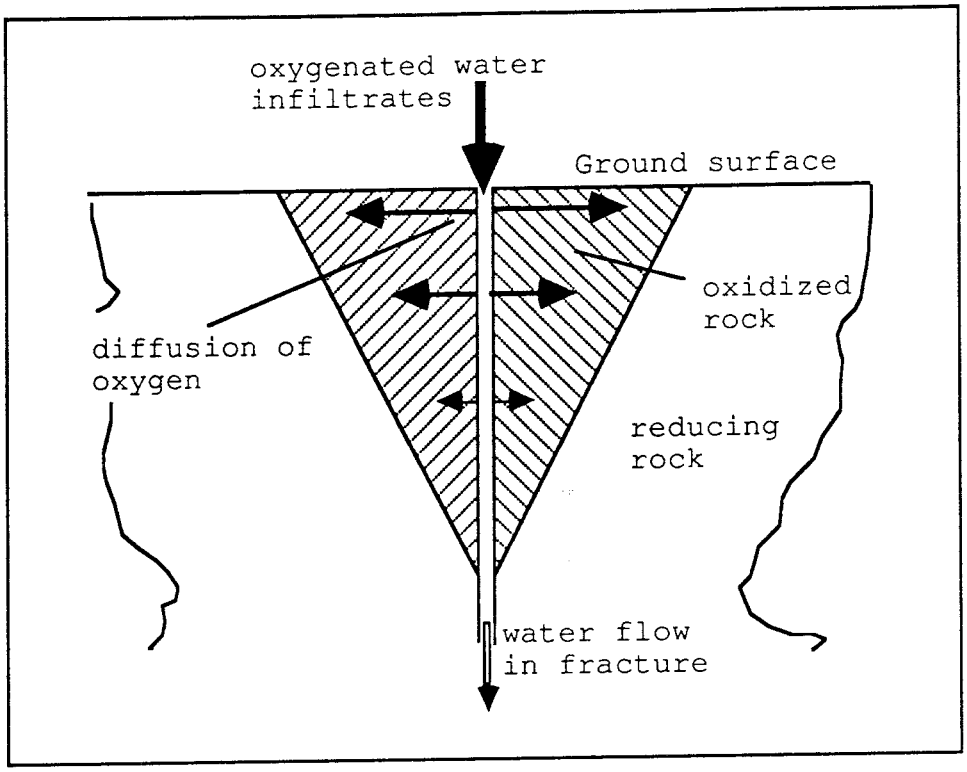

Figure 4-2 Development of redox front along a fracture or channel seen from the side.

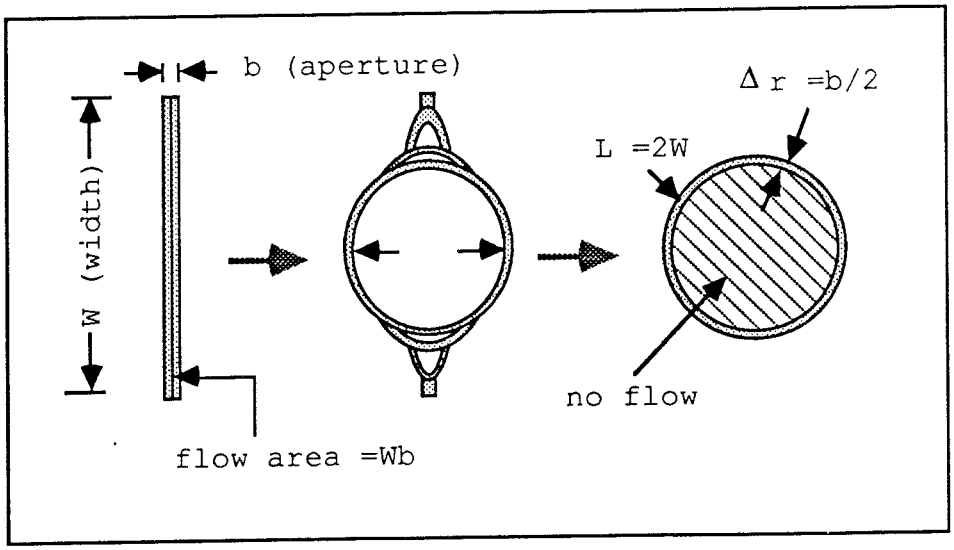

Figure 4-3 Obtaining an annulus from the expansion of a fracture. Slit and cylinder has the same wetted surface.

The rock is assumed to contain a large number of channels. The channels may have different flowrates and widths. Figure 4-4 shows a cross-section of rock with independent channels. Every channel has on the average a cross-section of rock which may be oxidized by oxygen diffusing from that channel. The channels are independent for some distance but otherwise are part of a channel network.

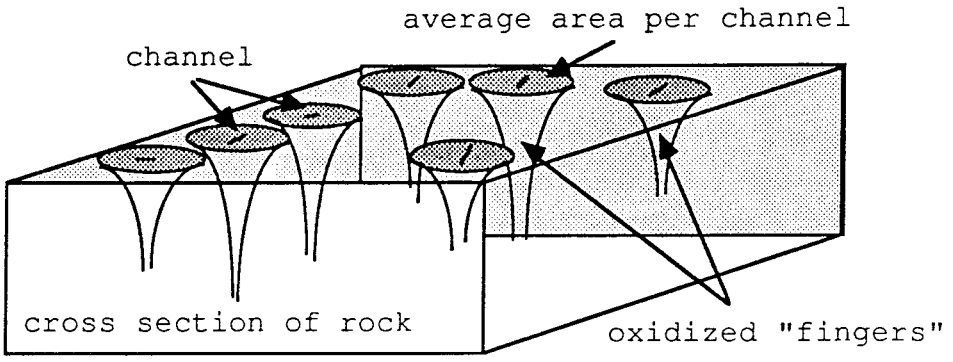

Figure 4-4 Cross-section of rock with independent channels.

4.2 THE MATHEMATICAL MODEL

The water flow is modelled as occurring through sparse channels in the rock. The oxidation of pyrite by oxygen is considered as the dominating reaction. It is assumed that this reaction is very fast such that O_2 and FeS_2 cannot coexist and a very sharp redox front is formed, separating the reducing zone from the oxidized zone.

The model considers advective transport of oxidizing water and diffusion of the dissolved oxygen into the rock matrix where the oxygen reacts with the pyrite. See Figure 4-2.

The governing equations, neglecting the axial dispersion in the fracture, are similar at those used by Neretnieks (1983). Then the governing equation for the advection transport of the species along a fracture or annulus is

$$\frac{\partial c}{\partial t} + v\frac{\partial c}{\partial z} + \frac{f}{m}\frac{\partial q}{\partial t} = 0 \qquad (4.1)$$

where the last term accounts for the diffusion into the rock, c is the concentration of oxidant within

the fracture, v is the velocity of the water, f is a stoichiometric factor, q is the average concentration of the oxidized, reducing species (FeS_2), and m is the ratio of water volume in the fracture to the solid volume of the rock.

The transport rate of the species at the moving boundary at distance r_b is

$$N = -\frac{dc}{dr}\Big|_{r_b} D_p \varepsilon_p A \qquad (4.2)$$

From a mass balance ($N = Aq_o f(dr_b/dt)$) the rate of movement of the redox front around a fracture or annulus is found

$$\frac{dr_b}{dt} = -\frac{D_p \varepsilon_p}{q_o f} \frac{\partial c_p}{\partial r}\Big|_{r_b} \qquad (4.3)$$

The diffusion equation in the rock is

$$\frac{\partial c_p}{\partial t} = \frac{D_p \varepsilon_p}{r^\alpha} \frac{\partial}{\partial r}\left(r^\alpha \frac{\partial c_p}{\partial r}\right) \qquad (4.4)$$

where $\alpha = 0$ for linear geometry and $\alpha = 1$ for cylindrical geometry. The product of the pore diffusivity and porosity ($D_p\varepsilon_p$) is the effective diffusivity, r is the distance from the center of the slab or annulus, r_b is the location of the redox front, and c_p is the concentration of oxidant within the pores of the rock.

Neretnieks (1983) showed that if the capacities of the pore liquid for holding the diffusing species are negligible compared to the reaction capacity of the solid, then the transport into the porous medium may be modelled as a semistationary process with a moving boundary. This assumption allows the term of accumulation $\partial c_p/\partial t$ in the diffusion equation, Equation (4.4), to be neglected.

4.2.1 Linear geometry

The diffusion mechanism may be modelled as diffusion from both sides into a slab of thickness S as shown in Figure 4-5.

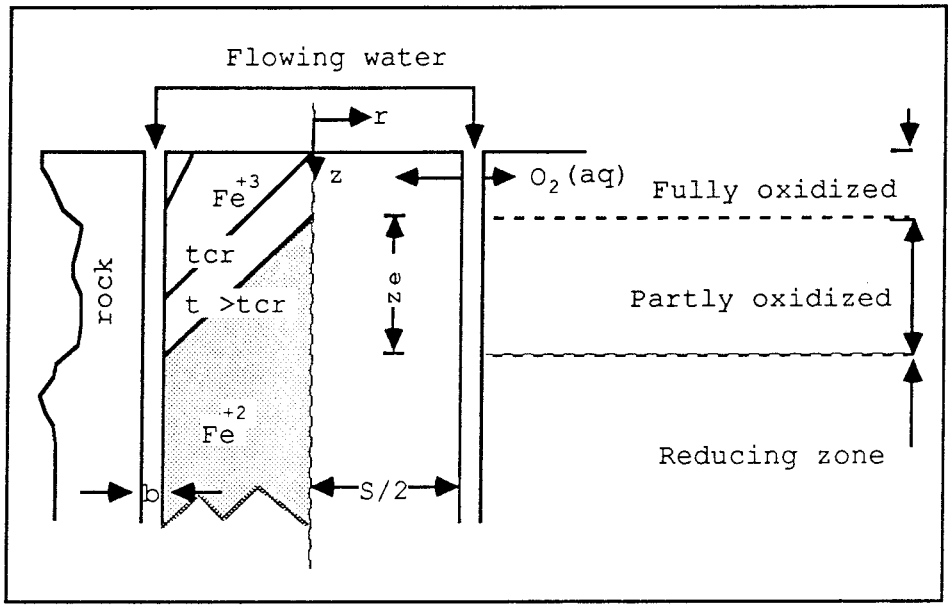

Figure 4-5 Representation of the model in linear geometry.

The following initial and boundary conditions are used

$$\text{IC} \quad c = 0 \quad \text{at} \quad t=0,\ z \geq 0$$

$$c_p = 0 \quad \text{at} \quad t=0,\ z \geq 0 \text{ and } r \leq S/2 \qquad (4.5)$$

$$q = 0 \quad \text{at} \quad t=0,\ z \geq 0 \text{ and } r \leq S/2$$

$$\text{BC} \quad c = c_o \quad \text{at} \quad z=0,\ t >0$$

$$c = 0 \quad \text{at} \quad z=\infty,\ t >0 \qquad (4.6)$$

$$c_p = c_s \quad \text{at} \quad r = S/2\ ,\ t >0$$

$$c_p = 0 \quad \text{at} \quad r=r_b\ ,\ t >0 \qquad (4.7)$$

where c_s is the concentration of oxygen at the wall of the fracture. Dimensionless variables are introduced

$$Q = \frac{q}{q_o} \quad , \quad C = \frac{c}{c_o} \quad , \quad \theta = D^* (t - \frac{z}{v}) \quad , \quad Z = \frac{D_p \varepsilon_p}{(S/2)^2 \, mv} z \qquad (4.8)$$

with

$$D^* = \frac{D_p \, \varepsilon_p \, c_0}{(S/2)^2 \, f q_0} \qquad (4.9)$$

where c_o is the concentration at the inlet of the fracture, q_o is the original concentration of the reducing species (or maximum amount of pyrite) to be oxidized.

Neretnieks (1983) obtained an analytical solution to this model in terms of the dimensionless variables above. Two cases may be distinguished, before and after the redox front has reached the center of the slab at the surface. The time to reach the center of the slab is defined as the critical time (t_{cr}).

$$t_{CT} = \frac{1}{2 D^*} = \frac{f q_0}{2 c_0} \frac{(S/2)^2}{D_p \, \varepsilon_p} \qquad (4.10)$$

The respective solutions are:

$$Q(\theta, Z) = \sqrt{2 D^* t} - Z \qquad \theta \leq 1/2 \qquad (4.11)$$

$$Q(\theta, Z) = \theta - Z + \tfrac{1}{2} \qquad \theta > 1/2 \qquad (4.12)$$

where $\theta = 1/2$ is the value of the dimensionless critical time.

4.2.2 Cylindrical geometry

The system under study includes the semi infinite porous rock volume extending from $z \geq 0$ and $r \geq r_o$. In this volume there is a vertical cylindrical annulus where a fluid flows. As above the fluid has a concentration c of a reactive substance (the oxidizing species) and the porous solid has a

concentration q_o (which is defined later as the maximum concentration to oxidize) of a substance (the reducing solid) with which the solute reacts. The oxidizing species may diffuse into the porous solid to react with the reducing species. The reaction is so fast that it may be seen as instantaneous.

The same nomenclature that was used above to describe the linear geometry, will be used here.

The diffusion equation, Equation (4.4), for cylindrical geometry $\alpha = 1$, is evaluated for the boundary conditions, where r_o is the radius of the hole

$$\text{IC} \quad \begin{aligned} c &= 0 \quad \text{at} \quad t=0,\ z \geq 0 \\ c_p &= 0 \quad \text{at} \quad t=0,\ z \geq 0 \text{ and } r \geq r_o \\ q &= 0 \quad \text{at} \quad t=0,\ z \geq 0 \text{ and } r \geq r_o \end{aligned} \tag{4.13}$$

$$\text{BC} \quad \begin{aligned} c &= c_o \quad \text{at} \quad z=0,\ t>0 \\ c &= 0 \quad \text{at} \quad z=\infty,\ t>0 \end{aligned} \tag{4.14}$$

$$\begin{aligned} c_p &= c_s \quad \text{at} \quad r = r_o \ , \ t>0 \\ c_p &= 0 \quad \text{at} \quad r=r_b \ , \ t>0 \end{aligned} \tag{4.15}$$

and with the assumption of a semistationary process, $(\partial c_p/\partial t = 0)$ then

$$\frac{\partial c_p}{\partial r} = \frac{\partial c_p}{\partial r}\Big|_{r_b} = \frac{-c_s}{r_b \ln(\frac{r_b}{r_o})} \tag{4.16}$$

Inserting this equation into the rate of the redox front movement described by Equation (4.3), gives

$$\frac{dr_b}{dt} = \frac{D_p \varepsilon_p}{q_o f} \frac{c_s}{r_b \ln\left(\frac{r_b}{r_o}\right)} \qquad (4.17)$$

If it is assumed that there is not film resistance (Bi -> ∞) to simplify the development of the equations, then $c_s(r=r_o) = c_o$ at the ground surface, z=0. The location of the redox front (r_b) at the surface, is determined by integration of Equation (4.17) from $r = r_o$ to $r = r_b$. This is valid for times less than the critical time which is defined as the time at which the redox front reaches the outer radius (r_{out}) at the surface of the ground level, z=0. This would be when the fronts from two channels meet.

$$\frac{r_b^2}{2} \ln\left(r_b / r_0\right) + \frac{r_0^2 - r_b^2}{4} = A^* t \qquad (4.18)$$

Evaluating the above equation for $r_b = r_{out}$, the critical time is obtained

$$t_{cr} = \left(\frac{r_{out}^2}{2} \ln\left(r_{out} / r_0 \right) + \frac{r_0^2 - r_{out}^2}{4} \right) \Big/ A^* \qquad (4.19)$$

where A^* is defined as $(D_p \varepsilon_p c_o)/(q_o f)$. As in the linear geometry case [Neretnieks, 1983], the introduction of dimensionless variables transform the governing equations, Equations (4.1) and (4.17), in

$$\frac{dQ}{d\theta} = \frac{C}{\frac{B}{4} \ln\left(QB + 1 \right)} \qquad (4.20)$$

and

$$\frac{\partial C(Z,\theta)}{\partial Z} + \frac{\partial Q(Z,\theta)}{\partial \theta} = 0 \qquad (4.21)$$

with $B = (r_{out}/r_o)^2 - 1$. The dimensionless variable Z and D^* are redefined as

$$Z = \frac{D_p \varepsilon_p}{r_0^2 m v} z \qquad D^* = \frac{D_p \varepsilon_p c_0}{r_0^2 q_0 f} \tag{4.22}$$

for the cylindrical case.

The solution of the Equations (4.20) and (4.21) is obtained, following the same method used by Cooper and Liberman (1970), with boundary conditions such as $C = 1$ at $\theta \geq 0$, $C = 0$ at $z > 0$, and $Q = 0$ at $z \geq 0$.

Similar to the linear geometry case, we distinguish two cases:

a) At times less than the critical time

$$\frac{B}{4} \int_{Q(\theta,0)}^{Q(\theta,Z)} \frac{\ln (qB+1)}{q} dq = -Z \qquad \text{at } \theta \leq \theta_{cr} \tag{4.23}$$

The value of $Q(\theta,0)$ at the surface is calculated from Equation (4.20) with C=1

$$\theta = f(Q) = \frac{(QB+1)\ln (QB+1) - QB}{4} \tag{4.24}$$

b) At times larger than the critical time

$$\frac{B}{4} \int_{1}^{Q(\theta,Z)} \frac{\ln (qB+1)}{q} dq = \theta - \theta_{cr} - Z \qquad \text{at } \theta \geq \theta_{cr} \tag{4.25}$$

where the dimensionless critical time is obtained from Equation (4.24) evaluated for Q =1

$$\theta_{cr} = \frac{((B+1)\ln (B+1) - B)}{4} \tag{4.26}$$

No closed form integral of Equations (4.23) or (4.25) has been found. It will be solved by means of expressing the logarithmic function $\ln(qB+1)/q$ in terms of an infinite series. Two solutions are given, depending in the value of QB. Then the semianalytical solutions are

a) At times less than the critical time ($\theta \leq \theta_{cr}$)

for QB ≤ 1

$$\frac{B}{4}\sum_{0}^{\infty}\frac{(-1)^{(n+1)}}{n^2}\{[Q(Z,\theta)B]^n - [Q(0,\theta)B]^n\} = -Z \qquad (4.27)$$

and for QB > 1, we get

$$\frac{B}{4}\left\{\frac{[\ln(QB)]^2 - \{\ln[Q(0,\theta)B]\}^2}{2} + \sum_{0}^{\infty}\frac{(-1)^n}{n^2}\{(QB)^{-n} - [Q(0,\theta)B]^{-n}\}\right\} = -Z \qquad (4.28)$$

b) The solutions after the critical time ($\theta > \theta_{cr}$), are

for QB ≤ 1

$$\frac{B}{4}\sum_{0}^{\infty}\frac{(-1)^{(n+1)}}{n^2}\{[Q(Z,\theta)B]^n - B^n\} = \theta - \theta_{cr} - Z \qquad (4.29)$$

and for QB > 1, we get

$$\frac{B}{4}\left\{\frac{[\ln(QB)]^2 - [\ln(B)]^2}{2} + \sum_{0}^{\infty}\frac{(-1)^n}{n^2}[(QB)^{-n} - B^{-n}]\right\} = \theta - \theta_{cr} - Z \qquad (4.30)$$

Taking the derivative with respect to time of Equation (4.29) or (4.30), it is found that the redox front velocity after the critical time is constant

$$V_{front} = \frac{v}{1+\frac{q_0 f}{m c_0}} \qquad (4.31)$$

Combining Equations (4.20), (4.23), and differentiating the dimensionless variable θ, the velocity of the redox front along the z-axis before the critical time is obtained.

$$V_{front} = \frac{v}{1+\frac{q_0 f Q}{m c_0}} \qquad (4.32)$$

Where Q is measured at the surface of the ground, z=0.

The distance "z_e" along a annulus at which traces the oxygen just still can been found, i.e. the tips of the front, can be calculated from Equation (4.27) or (4.29).

$$z_e = \frac{r_o^2 m v}{D_p \varepsilon_p} \sum_0^{\infty} \frac{(-1)^{(n+1)}}{4 n^2} B^{(n+1)} \qquad (4.33)$$

4.3 CALCULATIONS OF THE MOVEMENT OF THE REDOX FRONT IN THE CHANNELLING CASE

There is no direct information on the flow rates in the fractures and fracture zones in the deeper lying rock at Poços de Caldas. Calculations have been made by Noy and Holmes (1987) based on the assumption of porous flow in a non fractured medium. The results show that the flowrates are quite variable and may locally be on the order of the rainfall and higher. The calculations do not account for fractures or for anisotropy of the hydraulic conductivity. The latter may be expected due to the preferential directions of the fracturing. The results can at best be used to obtain a rough estimate of the flowrates. We address the problem in several stages. To have some first basis for the calculations we assume that 0.1 $m^3/(m^2 \cdot a)$ oxygen equilibrated rainwater infiltrates into the ground to the depth of the redox front. We will later return to this assumption. With this assumption the rate of supply

of oxygen to the rock is known. This oxygenated water will divide itself between the different channels in the rock and also to some unknown extent flow in the porous matrix of the rock itself. The rock matrix above the redox front is more porous (20 %) than the unaltered rock (4 %) and can be expected to be more permeable.

Above the redox front a larger fraction of the flow can be expected to be in the matrix. Of all the infiltrating water then, an unknown fraction will flow in the rock matrix and in many small fractures. If the small fractures are near enough to each other then their redox fronts will meet and a continuous jagged front will form. This is illustrated in Figure 4-6.

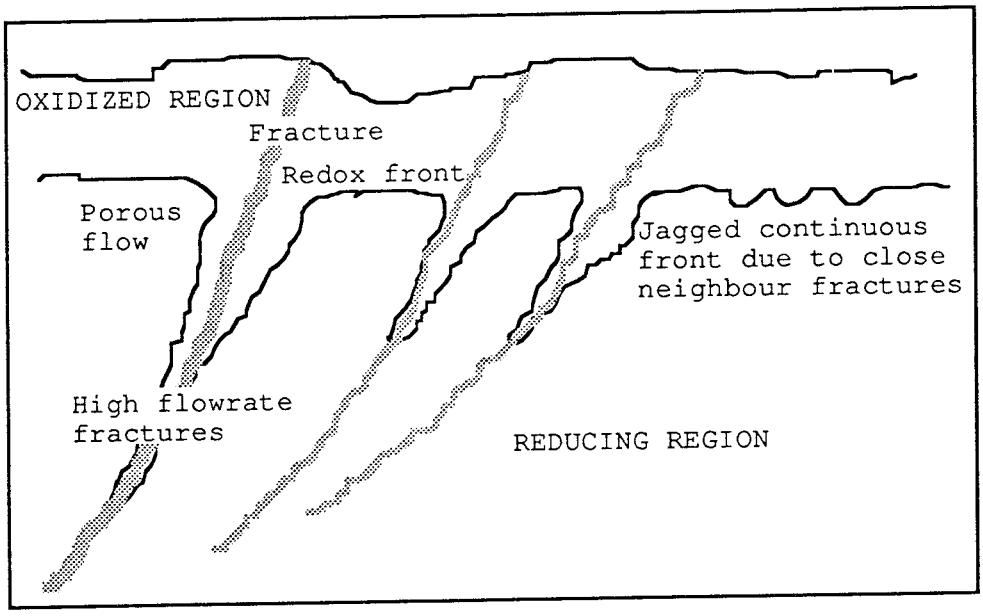

Figure 4-6 Development of redox front by porous flow and along channels.

Even if the total infiltrating flowrate to the redox front is known the fraction entering the larger channels is not known. The approach taken is to calculate the development of the front in channels with different flowrates of water, or more precisely, the flowrate of oxygen into the fracture, and compare with the observed extent of the redox fingers.

There is no information on widths, frequencies and flowrate distribution in channels in the rock of the uranium mine in PDC. There are, however, observations in several tunnels in crystalline rocks in Sweden which show that channel widths range from a few centimeter to tens of centimeters and up to

one meter. The frequency of channels range from 1 per 20 m^2 in Stripa [Abelin et al. 1985] to about 1 per 100 m^2 in SFR [Bolvede et al. 1987] and Kymmen [Palmkvist et al. 1987] in the good rock. In fracture zones in Kymmen the frequency was nearly one order of magnitude larger. The flowrates vary considerably between channels.

Table 4-1 shows the flowrate distribution found in the tunnels charted in SFR [Bolvede et al. 1987].

Table 4-1 Fraction of the total flowrate which flows in different categories of channels. The data are from SFR in a mapped area of 14000 m^2. Categories 7 and 8 are extrapolated for use at PDC.

Channel category	Relative flowrate	Fraction of spots	Fraction of flowrate	Flowrate per channel in PDC.* $[m^3/s]*10^6$
1	32	0.012	0.131	2.758
2	16	0.024	0.148	1.550
3	8	0.073	0.207	0.723
4	4	0.250	0.305	0.312
5	2	0.232	0.126	0.138
6	1	0.409	0.084	0.052
7	1/2			0.026
8	1/4			0.013

* These values give an average flowrate of 100 $l/(m^2 \cdot a)$.

In the field observations of channeling the distribution is truncated. In the SFR distribution for example the channel flowrates span only a flowrate range of a factor of 32. The histogram (SFR) also suggests that channels with smaller flowrates may exist. The number of these channels would have been large, but the total flowrate in them could still be small in comparison to the flowrate in the high flowrate channels. To the six channel categories in SFR two more categories with smaller flowrates have been added. In the computations, the assumed total infiltrating flowrate, 0.1 $m^3/(m^2 \cdot a)$, is divided up among the six original channel categories of SFR in proportion to their frequency. In addition, for other computations

the two additional channel categories have been assigned flowrates, each a factor of 2 smaller than the previous. In the calculations below each channel is treated as if it is independent of all others.

To calculate the movement of a redox front by channeling it is necessary that the geometrical characteristics of the channels, the flow distribution, and channel density are known. Having no site specific data, the calculations will be made using the relative SFR flowrate distribution applied to the conditions at the uranium mine.

The relative flowrate distribution among the channels is thus given. The absolute flowrate is one of the entities that will be sought. To begin with the absolute flowrate is assumed to be known and equal to 0.1 $m^3/(m^2 \cdot a)$. The consequences of this assumption, as to the rate of movement of the redox fingers are then explored and if necessary the overall flowrate can be adjusted.

4.3.1 General assumptions

The redox front develops out from a fracture or a channel like a growing wedge or cone respectively. This is illustrated in Figure 4-7 below.

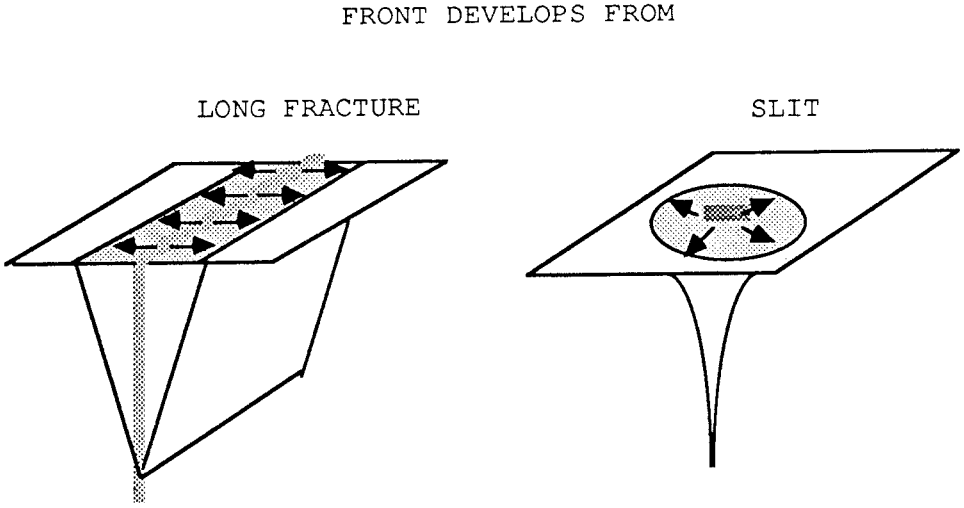

Figure 4-7 Development of redox front from a long fracture and from a narrow slit.

As the fronts grow further sideways they will eventually meet the fronts from neighbouring channels, Figure 4-8. At the mouth of the channel all fronts grow equally fast sideways irrespective of the flowrate into the channel. This implies that

if there is a large number of small channels the surface will all be oxidized quickly. It may be noted that in the present calculations the vertical diffusion of oxygen from the air is neglected. Zhu (1988) showed that this mechanism will allow for a much smaller rate of front growth than that due to the infiltrating water.

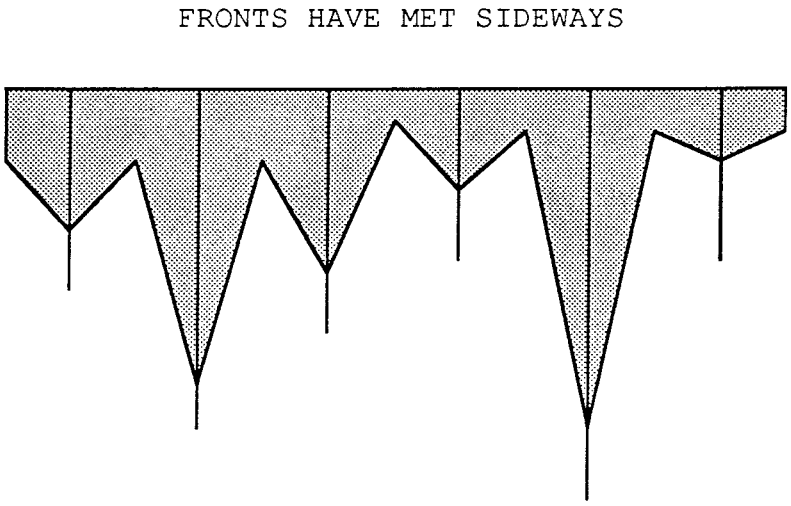

Figure 4-8 Fronts from adjacent channels have meet.

As a lower limit of the frequency of channels, the SFR data are used. At that site the six mapped categories have on the average one channel per 85 m^2. If the front around each channel spreads radially the radius will be 4.6 m to contain the redox front in the horizontal plane. If there were 4 times as many channels, including the small ones, the radius would be 2.3 m. For 16 times as many channels the radius would be 1.15 m.

The concentration of the dissolved oxygen in the intruding surface water is assumed to be c_o = 10 mg/l. This is the solubility of oxygen in water in contact with air at 20 °C, [Zhu, 1988]. It is assumed that above the bedrock there is no layer of soil which reacts with the O_2. The rock is thus, exposed directly to the atmosphere. The rock originally contains 2 % pyrite (by weight). It is assumed to have constant physical properties such as effective diffusivity $D_e=1.2*10^{-10}$ m^2/s and rock porosity $\varepsilon_p=0.15$ [Gidlund and Neretnieks, 1987]. For the stoichiometric factor f, a value of 15/4 is used, Equation (2.5).

The measured hydraulic conductivity of the rock ranges from 10^{-7} to 10^{-5} m/s. Thus, a $K_p= 3.0*10^{-6}$ m/s is considered and together with a hydraulic

gradient (i) of 10^{-3} m/m gives a Darcy velocity ($u = Kp*i$) of $3.0*10^{-9}$ $m^3/(m^2 \cdot s) \approx 0.1$ $m^3/(m^2 \cdot a)$. The infiltration water flowrate fluctuates into the range of 10 to 20 % of a rainfall of 1600 mm/a [Smellie et al. 1987]. The assumptions are tabulated in Table 4-2.

Table 4-2 Data used in the calculations

W	Channel width	1	[m]
b	Fracture aperture	$1*10^{-3}$	[m]
S	Spacing of fractures	85	[m]
r_o	Annulus radius	0.31	[m]
r_{out}	Outer radius	4.61	[m]
	Channel density	1/85	[spot/m^2]
c_o	Oxygen concentration	$3.13*10^{-4}$	[mol/l water]
D_p	Pore diffusivity	$8.0*10^{-10}$	[m^2/s]
ε_p	Porosity	0.15	[-]
f	Stoichiometric factor	3.75	[-]
q_o	Pyrite concentration	0.35	[mol/l rock]
Kp	Hydraulic conductivity	$3*10^{-6}$	[m/s]
i	Hydraulic gradient	$1*10^{-3}$	[m/m]

4.3.2. Results

For the cylindrical geometry (Figure 4-3), the ratio of fluid to the solid, "m", was redefined as $Wb/(r^2_{out}-r^2_o)/\pi$, where the area of the fracture perpendicular to the flow is "Wb". The equivalent annulus that results from a fracture with the given dimensions (aperture b = 10^{-3} m, width W = 1 m), has a radius of 0.31 m. The outer radius that results from the condition of 1 channel per 85 m^2, is 4.61 m

Some particular results are tabulated in Table 4-3. Figures showing the results for both linear and cylindrical geometry and different channels are included in the appendix.

From Table 4-3, it is observed that the linear geometry would require a very long time (10^9 years) for the front from a channel to reach the front from the other channels at the surface (critical time). This means that times larger than 10^9 years are needed to oxidize the whole area of the surface. For

the cylindrical approach the critical time is $26*10^6$ years. The velocity of the redox fronts at critical time are quite similar for both approaches. At a given time the length of the redox "finger" is larger for the linear case (about 3 times larger than the cylindrical case at time of $26*10^6$ years). The oxidized volume of rock for both approaches is, of course, identical at a given time, since both are determined by the volume of oxygen equilibrated water infiltrated.

The results below are presented using the calculations for cylindrical geometry. Most of the discussion below is made using results for the channels with the largest flowrate but a similar trend is observed for the other channels.

Figure 4-9 shows the critical time as a function of distance that the redox front needs to cover, to reach the front from other fractures. It is observed that the critical time is strongly increased with the location of the outer boundary. If the border is situated at 4.6 m the critical time is $26*10^6$ years, while if the border is located at 2.3 m this time is $5.1*10^6$ years. The critical time is inversely proportional to the frequency of channels, irrespective of size. Critical times are also shown for other values of the parameters. This is made by calculating the critical time for different values of A^*, see Figure 4-9. This critical time is inversely proportional to the effective diffusivity and concentration of oxygen dissolved in the water.

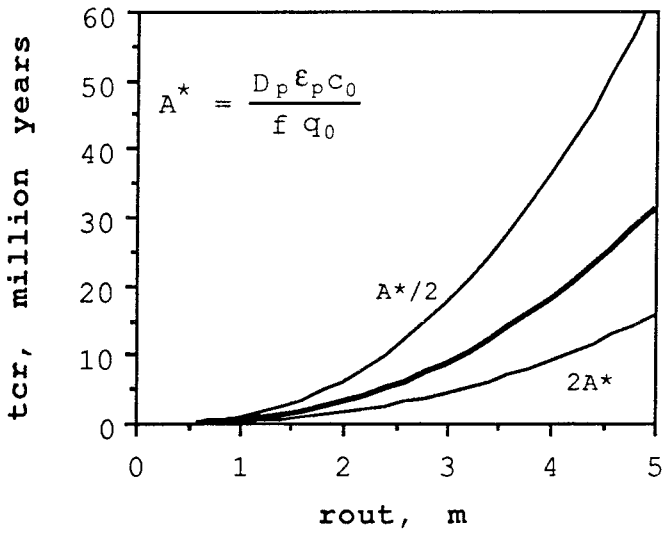

Figure 4.9 Outer radius vs. critical time. For different values of A*.

Table 4-3 Some results for the linear and cylindrical model for the channel of largest (I) and smallest (VI) channel velocity.

	Linear		Cylindrical	
Channel category	I	VI	I	VI
Water velocity, $[m/a]*10^{-3}$	86.5	1.64	86.5	1.64
Critical time, [million years]	1000		26	
Redox-velocity (z-axis) at t_{cr}, $[m/a]*10^{4}$	2.4	0.046	3.1	0.059
Length at 26 million years, [km]	78.3	1.49	28.9	0.55
Length at its respective t_{cr}, [km]	486.0	9.23	28.9	0.55
Oxidized volume at t_{cr}, $[m^3]* 10^{-6}$	20.7		5.31	
Length at 10^9 years, [km]	486.0	9.23	331.0	6.3
Oxidized volume at 10^9 years, $[m^3]* 10^{-6}$		20.7		20.7

Figure 4-10 shows the velocity (z-axis) of the redox front, computed in the fracture, as a function of the fraction of rock oxidized on the surface at time less than the critical time, Equation (4.32). At times greater than the critical time the front velocity is constant, Equation (4.31). The redox front velocity (z-axis) is for both geometries inversely proportional to the advance of this redox in the rock matrix, which is determined by the ratio

of the oxidized fraction (Q) evaluated at z equal to zero, Equation (4.32). This figure also shows the variation of the velocity of the redox front with respect to certain physical properties grouped in "kon1". The velocity of the redox front is increased with an increase of the oxygen concentration of the infiltrated water.

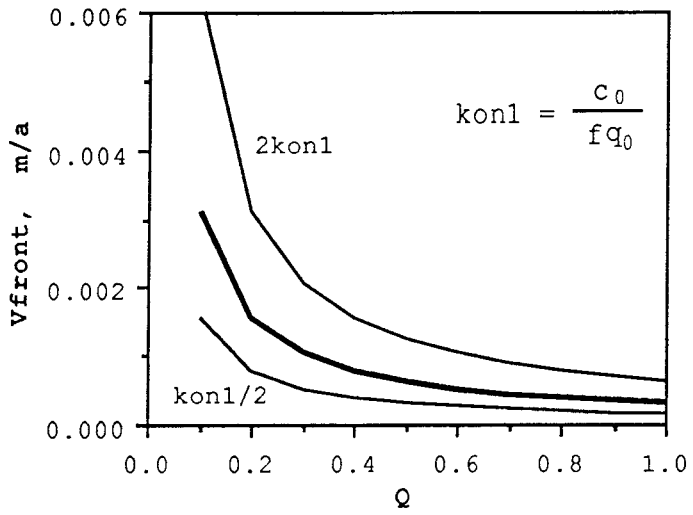

Figure 4-10 Velocity of the redox front (computed at its peak in the fracture or channel as a function of the fraction of oxidized rock computed at the surface of the ground, z = 0.

The development of the redox front in time is shown in Figure 4-11. The location of the redox front is shown as a function of the fraction of rock oxidized for different values of the group of parameters "kon2". The relationship between the fraction of rock oxidized at the surface and the time is shown in Figure 4-12.

Figure 4-13 shows, the length of the redox "fingers" at different fractions of the critical time. The linear and the cylindrical geometries showed a clear difference in the advance-form of the reaction plane. For the linear geometry these curves are straight lines (See Figure 5 in Appendix).

Figure 4-14 shows the movement of the redox front expressed in the length reached by its peak after the critical time. The location of the redox front varies linearly with time because the velocity of the front is constant after the critical time.

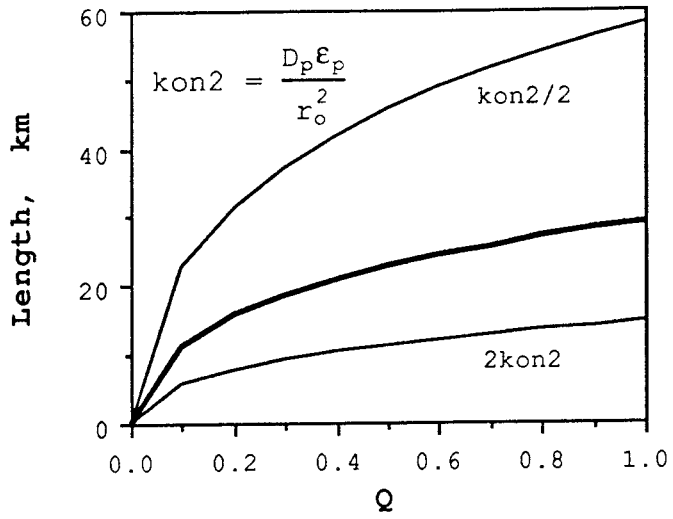

Figure 4-11 Length reached by the peak of the redox front along the wall of the fracture or annulus vs. fraction of the oxidized rock computed at the surface of the ground, z = 0.

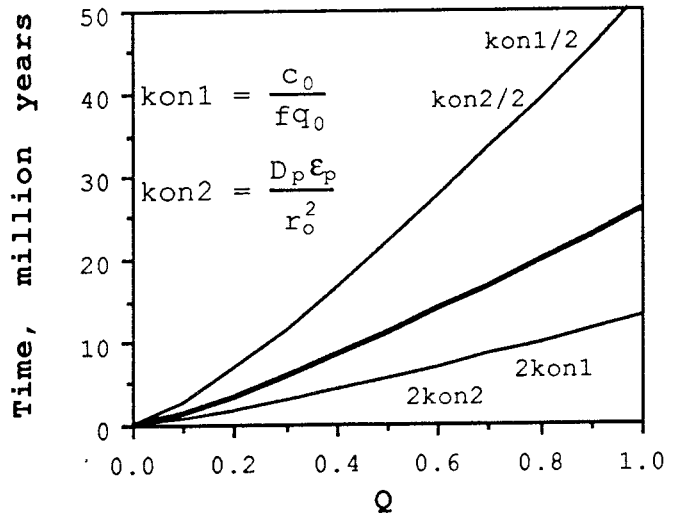

Figure 4-12 Time vs. fraction of oxidized rock reached at the surface of the ground, z = 0.

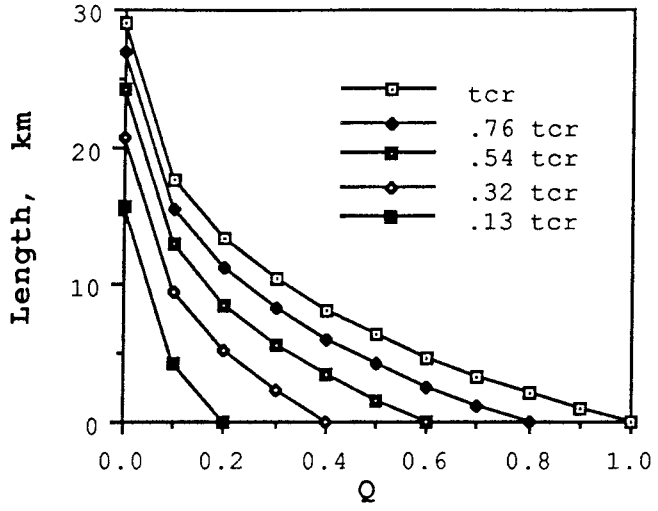

Figure 4-13 Length of the redox front vs. fraction of oxidized rock computed at the surface of the rock, for different fractions of critical time.

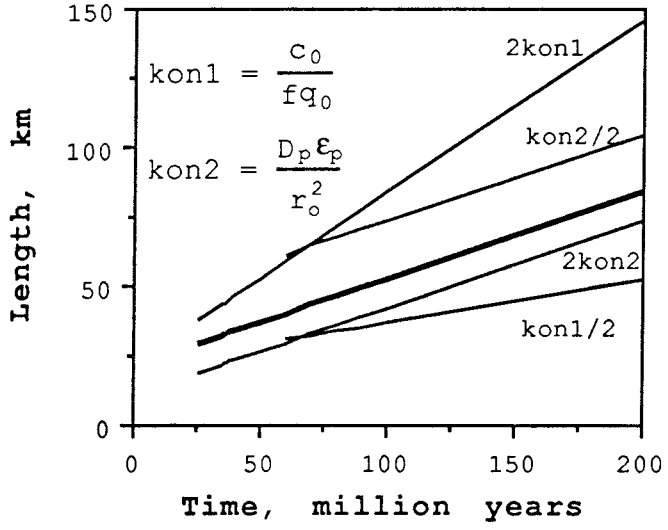

Figure 4-14 Length reached by the peak of the redox front after critical time vs. time.

4.3.3 Discussion of the constant flowrate channel assumptions

There are many unknown factors which may strongly influence the movement of the redox front, such as the flow distribution and the density of channels. These entities are very important when the movement of the front is calculated. Parameters such as the conductivity and gradient hydraulic (Kp,i) which are not constant with depth, could have a large influence on the redox front when this reaches large depths. The hydraulic conductivity and hydraulic gradient usually decrease with depth causing the flowrate to decrease. Furthermore streamlines tend to change from near vertical to horizontal with depth and then turn upward.

Obviously the above assumptions lead to impossible results. The redox front reaches depths of many km in the calculations whereas in reality hundreds of meters are reached.

There are several assumptions with are not reasonable. These will now be addressed and tested. One is that there was no erosion in the above calculations. Another is that a channel has the same properties over very long distances and that the flowrate is constant irrespective of depth.

Also, the physical properties of the rock that are variable (D_p,ε_p), could influence the movement of the redox front. The diffusive movement of the redox front into the rock matrix may be strongly affected. The effect of varying these parameters is, however, less than the effect that could be caused by a smaller hydraulic conductivity or a larger channel density.

After the matrix between fractures or annulus has been fully penetrated, the assessment of the redox front movement is similar whether the rock is considered as fracture or not (Zhu, 1988). The results of the velocities and lengths reached by both geometries in the time-interval after critical time, are equal if they were calculated by flow in porous rock because the m-value is << 1. See Equation (4.31).

5 MODELLING OF THE REDOX FRONT. ACCOUNTING FOR EROSION

As it was described before, the erosion is estimated to be of the order of many kilometers during the time in which the rock was oxidized. This means that the depth of the redox front is reduced by the erosion. For channels with small flow, a steady state may be established between the movement of the redox front and the erosion. The solution of the equations including the effect of the erosion were solved numerically. A constant erosion rate of 50 m per million years was used in the sample calculations.

The Crank-Nicolson implicit finite difference scheme was been used for the solution of the governing equations, Equations (4.1) and (4.17). The coupled system is solved iteratively. Because the mass of oxidant in the fracture is negligible if compared with the mass of oxygen which reacts with the pyrite, the numerical solution became unstable. The numerical scheme was rearranged to increase the stability of the system. The numerical code worked well, but the computing time was quite long.

To improve the numerical scheme another method was tested which neglectes the small capacity of the fracture to hold oxygen. A quasi steady state method was used for the concentration in the fracture. This means that the accumulation term in the Equation (4.1) which describes the concentration in the fracture, is neglected. Then an ordinary differential equation is solved for the concentration in the fracture. From these concentrations the diffusion into the rock matrix is then calculated for a time interval assuming that the concentration in the fracture in each node is constant during this time interval. The method works very well and the computing time was significantly reduced.

5.1 RESULTS AND DISCUSSION

The accuracy of the numerical model, not accounting for erosion, was tested with the analytical solution where the results obtained by both models was very similar.

The above calculations were based on the assumption that channels extend forever with the same flowrate all along and for all times. This is not a reasonable assumption for long distances, because of the "network" structure of channels, and because flowrates decrease with depth.

It is seen from Figure 5-1 that for channels with little flow, categories 6-8, the redox front in independent channels would stabilize at 20-200 m below the constantly eroding ground surface. For the channels with larger flowrates the length of the oxidized channels would become very large. It is conceivable that channels would keep their identity for tens to hundreds of meters because the channels are sparse. For larger distances the channels are bound to intersect other channels and form a network. This would lead the water in different channels to mix their waters and the channels would loose their identity. The fronts would not penetrate as far as the individual channel concept would indicate.

Furthermore, the flowrate at larger depths will decrease and also become more horizontal before finally turning upward. Very long "channels" will thus come up to the surface.

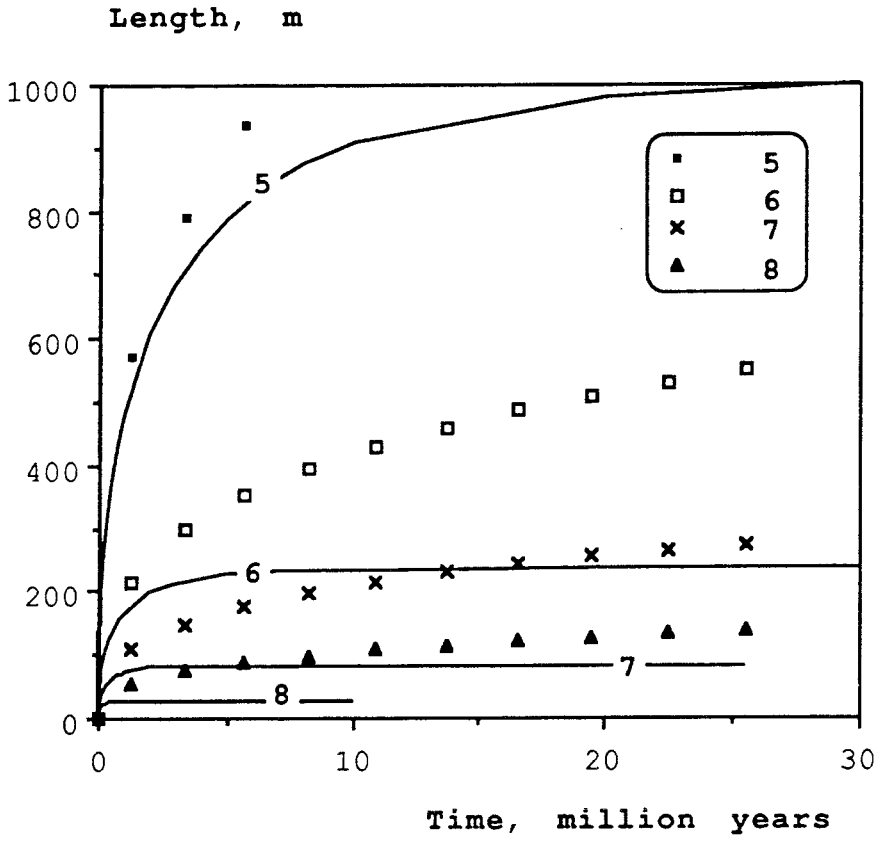

Figure 5-1 Length of oxidized "fingers" as a function of time considering no erosion and considering erosion (full lines) for independent channels. The number are flow categories of Table 4-1.

6 MODELLING OF THE REDOX FRONT BY CHANNELLING ACCOUNTING FOR EROSION AND VARIABLE INLET FLOWRATE

The conceptual model and the methodology used to solve the governing Equations (4.1) and (4.17), are the same that was used in chapter 5. The difference is that here, we introduce variable inlet flowrate. The physical basis for this is that after some erosion has taken place the upper part of channel network has eroded away and new inlets to the network are exposed.

The handling of this new introduction to the model, is made by randomizing the inlet flowrate among the six first categories of channels according its density distribution as is tabulated in Table 4-1.

Two types of calculations were made. In the first, it is assumed that the condition of change of inlet flowrate takes place every one hundred thousand years, and in the other case, the change of inlet flowrate occurs every one hundred meters of advance of the peak of the redox front.

The numerical method applied here, assumes that the capacity of the fracture to hold oxygen is very small and therefore a quasi steady state is applied to solve Equation (4.1) for a cylindrical geometry.

6.1 RESULTS AND DISCUSSION

Calculations were made up to 80 million years using 100 channels.

The results for the first case are shown in Figure 6-1. Obviously the lengths of the channels are far to large. This is because the channel with high flowrate strongly influences the advance of the redox front. The erosion then does not play a large roll as it does with lower flowrates.

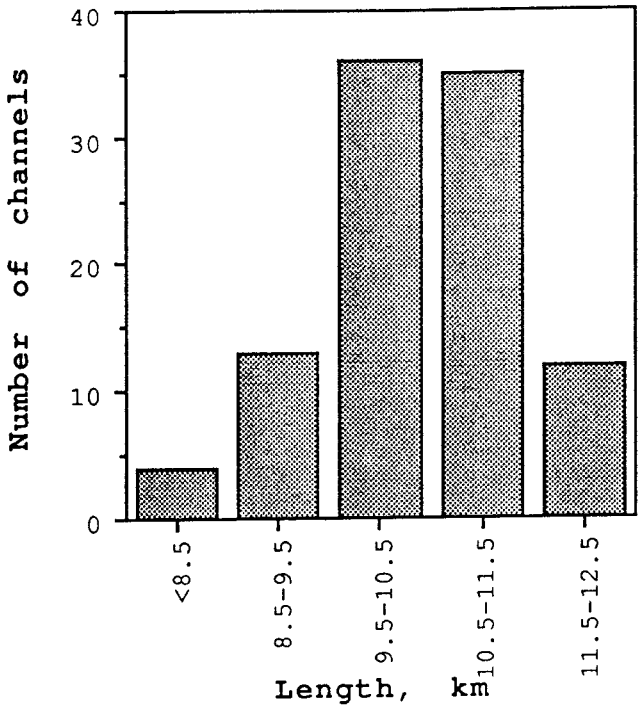

Figure 6-1 Histogram of number of channels vs. length of the redox "fingers" for changes in flowrate every 100 thousand years.

In the other case the channel property (flowrate) changed every time 100 m of rock had eroded away. The results are shown in Figure 6-2.

From the Figure 6-2, we can deduce that the effect of channels with high flowrates is limited by the condition assumed (changes each 100 meters of advance of the redox front). Then the advances of the peak of the redox front when the channel has high flowrate, is broken at very short time, and the movement of the redox front tends sometimes to a stationary state by effect of the erosion when the channel has the lower flowrates.

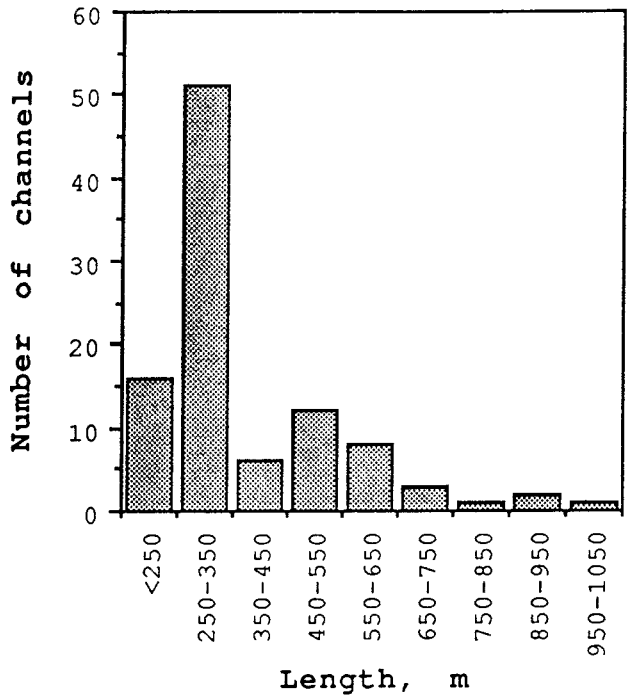

Figure 6-2 Histogram, number of channels vs. length of the redox "fingers" for changes of flowrate every 100 meters of advance of the peak of the redox front.

In our calculations the changes of flowrates occur when the peak of the redox front has advanced 100 meters (stationary coordinate system). If the change of the flowrate occurs when the depth of the front is increased by 100 meters (related to a moving coordinate system), all the channels tend to stabilize at a depth of about 200 meters. This is because a steady state condition is obtained after a certain time when the lowest inlet flowrate is chosen. Then the advance of the redox front is stationary which means that the advance of the peak of the redox front and the advance of the erosion become to the equilibrium, and no more changes occur

7 DISCUSSION AND CONCLUSIONS

The data described and reported in the 3-D plots is a first attempt to bring the various data together in a more understandable and presentable form. The plots clearly show 3-D ragged fronts.

The histogram in Figure 3-4 shows the number of fingers with the depth, taking as reference level 1200 m over the sea level. No accounting for small fingers is made.

The frequency of channels found in the Swedish crystalline rocks was on the order of 1/20 m^2 to 1/100 m^2. The frequency of redox fingers at PDC was on the order of 1/1000 m^2. At PDC the fingers in the mined away rock could not be reconstructed. The figure for PDC is thus truncated and gives too few channels. The resolution of the PDC mapping is very coarse and finer channels will not be found. Visual observations in the vertical walls show many more fine channels but these have not been quantified in the histogram.

If there were no erosion and the channels extended "forever" with the same flowrate, the rate of movement of the tip of the redox front decreases inversely to the square root of time. This means that for a constant rate of erosion there will be a time at which the front moves as fast as erosion takes place. This is shown in Figure 5-1. In this figure we can see also the oxidized length along a channel for channels with little flow, categories 4 - 8. For example, the stationary length is 0.2 km for channels in category 6. The fastest channels would extend many kilometers if they were isolated. Even assuming that these channels are horizontal for long distances, the distance is too long to be reasonable even accounting for erosion.

When changes of inlet flowrate are considered after constant time periods, the advance of the redox front is not much influenced. This is because the effect of the channel with high flowrate is very pronounced, giving a fast advance of the redox front. The erosion effect is negligible. When the changes of inlet flowrate are made at every 100 meters of advance of the front, the high flowrates for the channel end after short time. Then, the total interval of time during which the channel has lowest flowrate is much larger than the active time of the channel having high flowrate. Thus the total advance of the redox front is lower.

The field data show that the upper part of the rock is totally oxidized. This would be explained by the

existence of a large number of channels which transport oxygen in this upper zone. Another reason would be that the channels form a channel network where the channels lose their identity.

NOTATION

A	Area	[m^2]
A^*	Group of variables	[m^2/a]
b	Aperture of the fracture	[m]
Bi	Biot number	-
c	Concentration of oxidant in liquid	[mol/m^3]
c_o	Concentration at the inlet of the annulus or fracture	[mol/m^3]
c_p	Concentration of oxidant within the pores of the rock	[mol/m^3]
c_s	Concentration at the surface of the annulus or fracture	[mol/m^3]
C	Dimensionless concentration	
D_p	Pore diffusivity	[m^2/a]
D*	Group of variables	[a^{-1}]
f	Stoichiometric factor for the oxidation reaction	-
kon1	Group of variables	-
kon2	Group of variables	[a^{-1}]
m	Ratio of fluid to the solid.	[m^3/m^3]
N	Mass flux of species	[mol/a]
q	Concentration of the reducing species in the solid	[mol/m^3]
q_o	Original concentration in the solid of the reducing species	[mol/m^3]
Q	Dimensionless concentration	-
r	Radius from center of the hole or distance measured from center of the slab	[m]
r_o	Radius of the hole	[m]
r_{out}	Outer radius of the system	[m]
r_b	Location of the redox front at surface	[m]
S	Thickness of the slab	[m]
t	Time	[a]
t_{cr}	Critical time	[a]
v	Velocity of the water in the hole or fracture	[m/a]
v_{front}	Velocity of the redox front (z-axis)	[m/a]
W	Width of the channel	[m]
z	Distance along the hole or channel	[m]
z_e	Distance along hole or channel of leading edge of redox front	[m]
Z	Dimensionless distance	-
ε_p	Diffusional porosity of rock	-

θ	Dimensionless time	-
θ_{cr}	Dimensionless critical time	-

ACKNOWLEDGMENTS

This work forms part of the international Poços de Caldas project, jointly funded by SKB (Sweden), Nagra (Switzerland), United Kingdom Department of the Environment, and the Department of Energy U.S.A. We wish to acknowledge the work of the many other Project Principal Investigators who have provided the data for this study.

REFERENCES

Abelin H., Neretnieks I., Tunbrant S., Moreno L. Final Report of the Migration in a single fracture - Experimental results and evaluation. Stripa Project Report 85-03. OECD/NEA, SKB, 1985.

Bolvede P., Christianson R. SKB Forsmarksarbetena SFR. Vattenförande sprickor inom lagerområdet. VIAK, Stockholm (in Swedish), Water bearing fractures in the repository area, 1987.

Cooper R.S., Liberman D.A. Fixed-bed adsorption kinetics with pore diffusion control, Ind. Eng. Chem. Fundam., **9**(4), p 620, 1970.

Gidlund J., and Neretnieks I. Porosity, hydraulic conductivity, and diffusivity measurements of samples from Poços de Caldas Project, Progress report March through May 1987. Stockholm, 1987.

Lei W. Thorium mobilization in a terrestrial environment, Thesis at the faculty of the Graduate School of Science at the New York University, 1984.

Neretnieks I. Some uses for natural analogues in assessing the function of a HLW repository. Chemical Geology, **55**, p 175 - 188, 1986.

Neretnieks I. The movement of a redox front downstream from a repository for nuclear waste. Nuclear Technology, **62**, p 110, 1983.

Noy D.J., Holmes D.C. Hydrogeological modelling of the Osamu Utsumi Mine. Poços de Caldas, Quarterly progress report, Sept. - Nov. 1987, 1987.

Palmqvist K., Stanfors R. The Kymmen power station TBM tunnel. Hydrogeological mapping and analysis. SKB Technical report, 87-26, 1987.

Smellie J., Barroso L., Chapman N. McKinley I., Penna E. The Poços de Caldas project Feasibility study, Final report, SKB, June 1986-1987, 1987.

Ulbrich H. Depth of erosion in the Poços de Caldas alkaline massif, Southern Brazil. Appendix 3 to PDC progress report Dec. 1988 - Feb. 1989, 1989.

Zhu M. Some aspects of modelling of the migration of chemical species in groundwater system, Licentiate thesis Dept. Chem. Eng. Royal Institute of Technology, Stockholm, Sweden, 1988.

APPENDIX

The subscripts "a,b" indicate, calculations made with the cylindrical and linear model respectively.

The thick line indicates, calculations made with the parameter found or assumed at PDC. (kon1, kon2, and A^*)

The kon1, kon2, and A^* are groups of parameters which were varied by a factor of 2 of the values which those groups have if they were calculated at conditions assumed at PDC.

Figures 2 to 5 show results calculated before critical time has been reached.

Figure 6 shows results calculated after critical time has been reached.

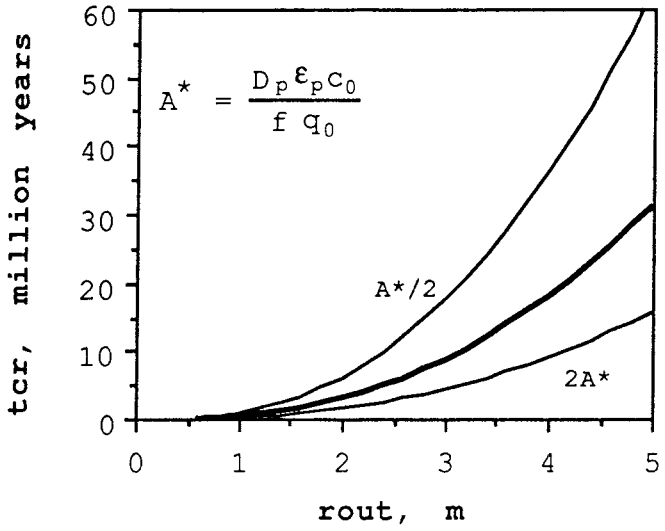

Figure 1-a Outer radius vs. critical time. For different values of A*.

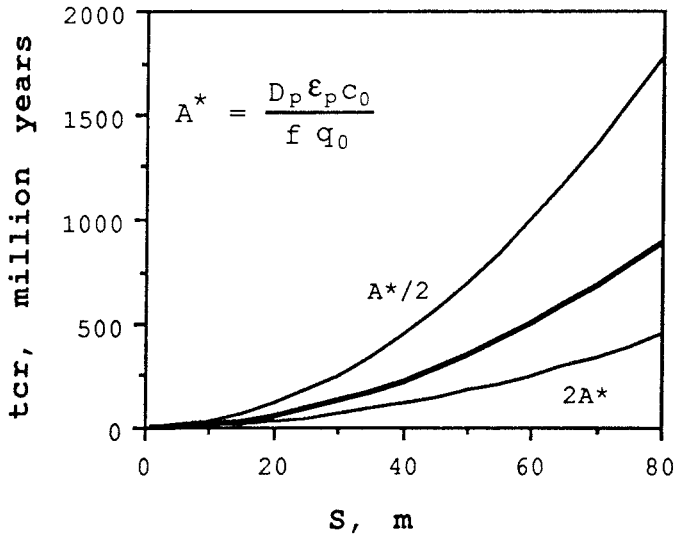

Figure 1-b Thickness of oxidized slab vs. critical time. For different values of A*.

Figure 2 Velocity of the redox front computed at the peak (along the wall of the channel or annulus) vs. fraction of oxidized rock computed at the surface of the ground, z = 0.

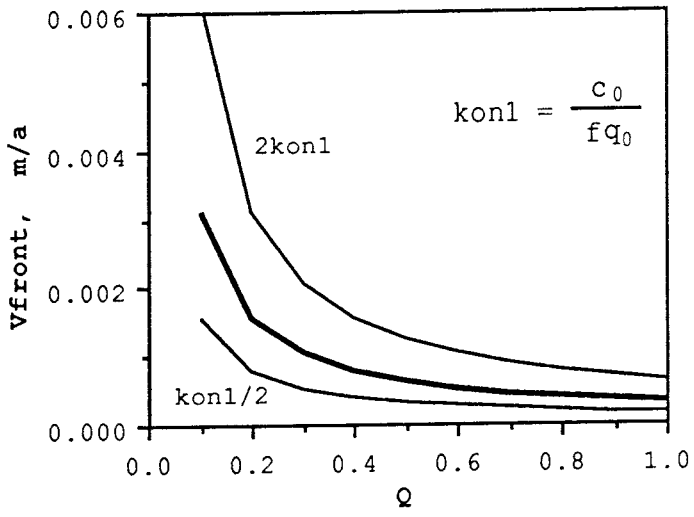

(2a)

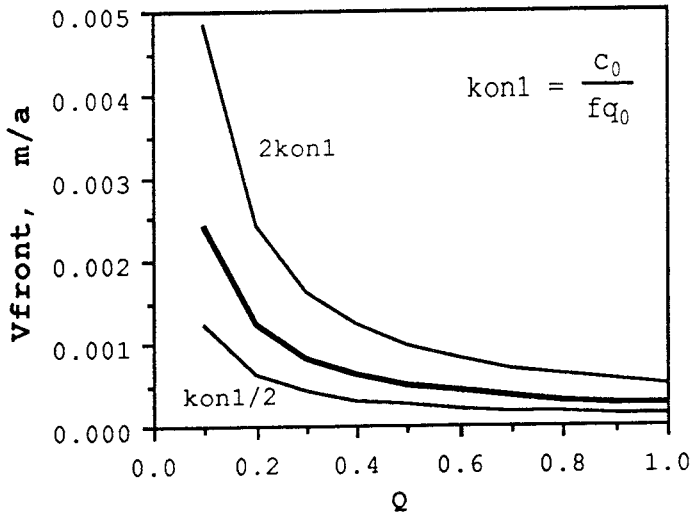

(2b)

Figure 3 Length reached by the peak of the redox front along the wall of the fracture or annulus vs. fraction of the oxidized rock computed at the surface of the ground, z = 0.

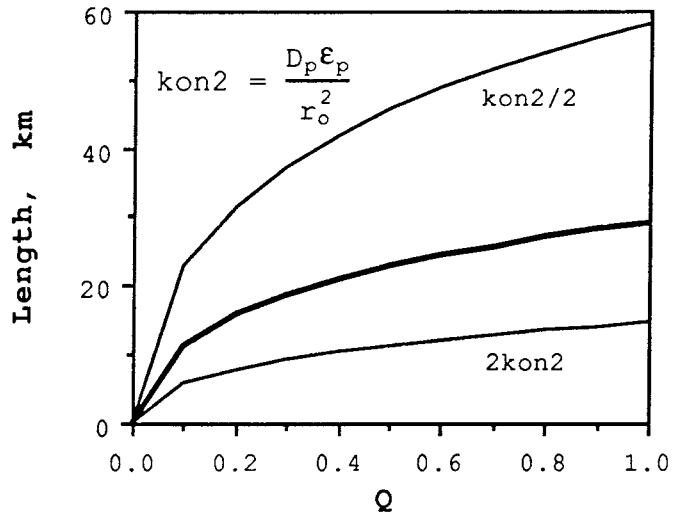

(3a)

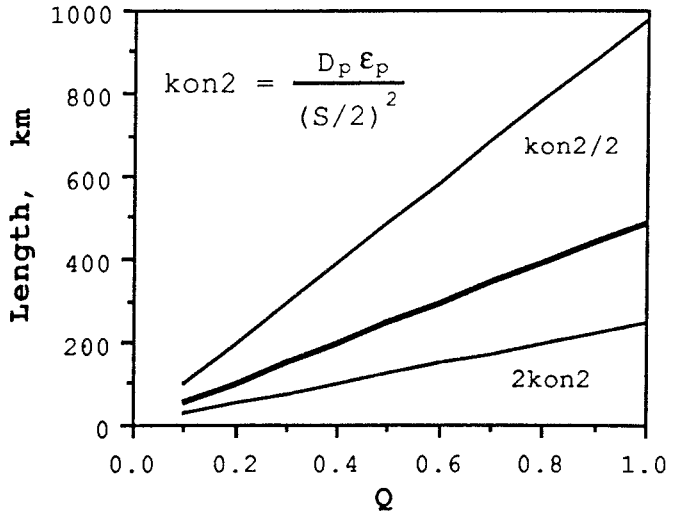

(3b)

Figure 4 Time vs. fraction of oxidized rock reached at the surface of the ground, z= 0.

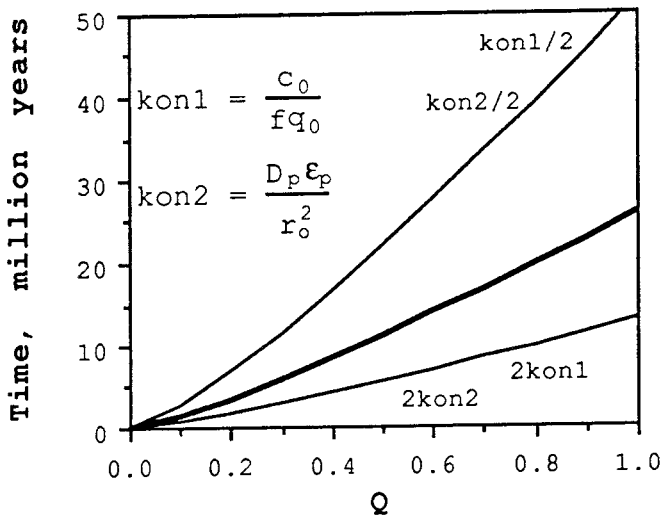

(4a)

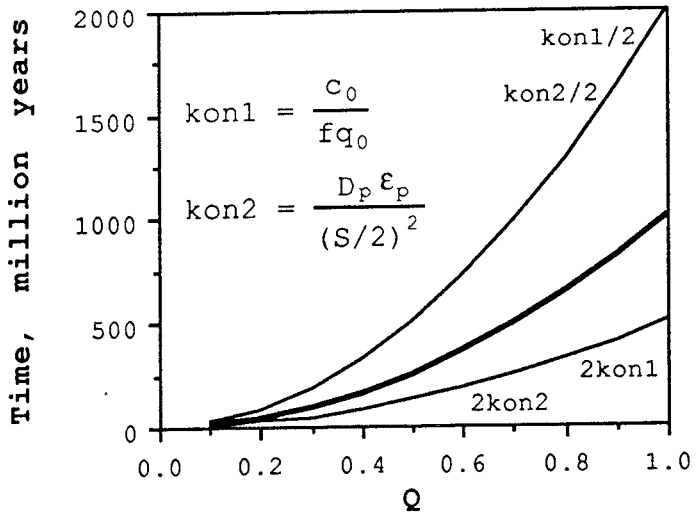

(4b)

Figure 5 Length of the redox front vs. fraction of oxidized rock computed at the surface of the ground, z = 0. For different fractions of critical time.

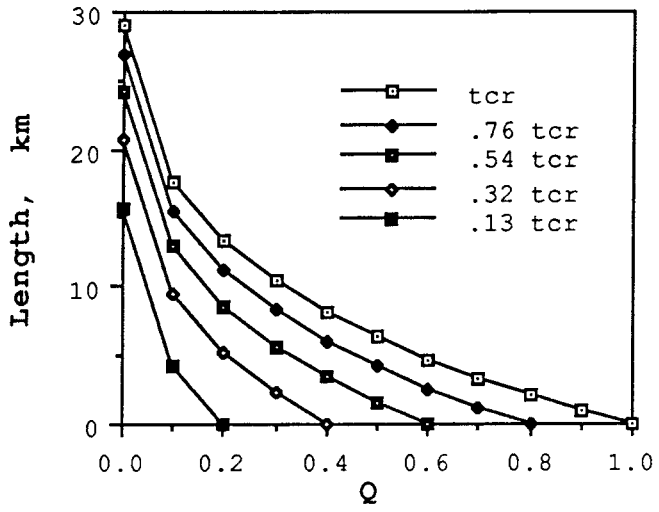

(5a)

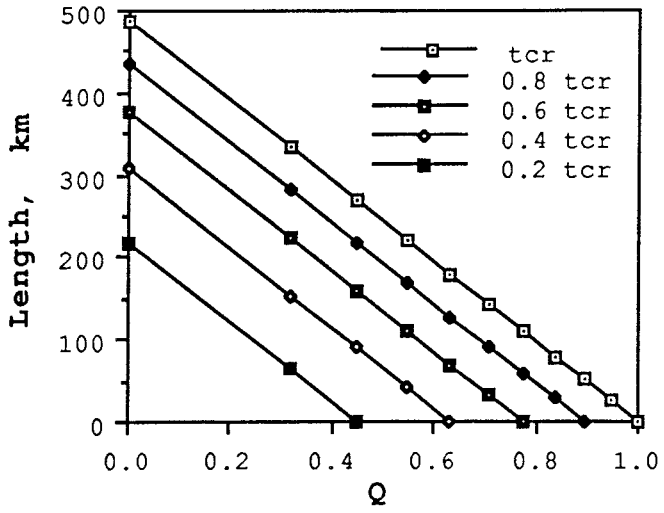

(5b)

Figure 6 Length reached by the peak of the redox front after critical time vs. time.

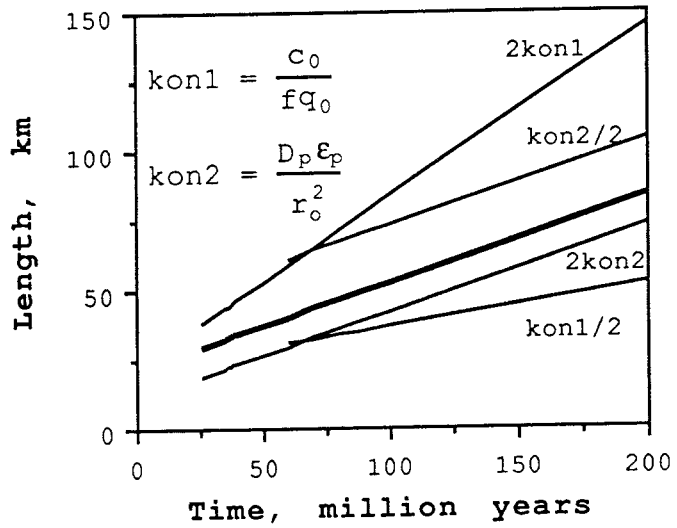

(6a)

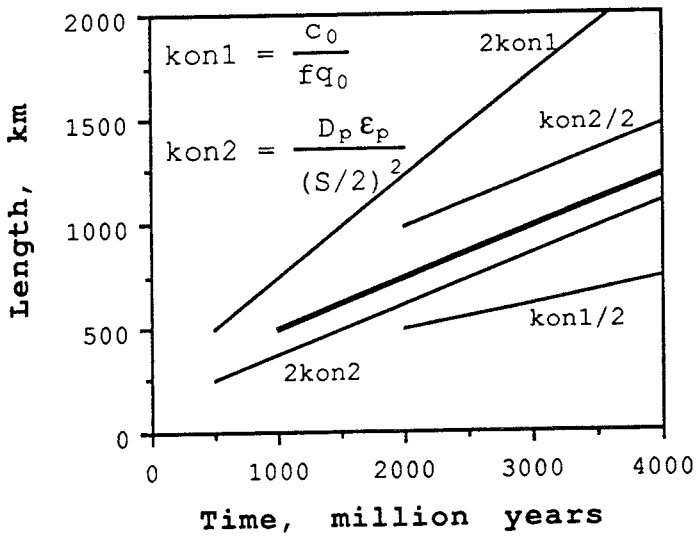

(6b)

List of SKB reports

Annual Reports

1977-78
TR 121
KBS Technical Reports 1 – 120
Summaries
Stockholm, May 1979

1979
TR 79-28
The KBS Annual Report 1979
KBS Technical Reports 79-01 – 79-27
Summaries
Stockholm, March 1980

1980
TR 80-26
The KBS Annual Report 1980
KBS Technical Reports 80-01 – 80-25
Summaries
Stockholm, March 1981

1981
TR 81-17
The KBS Annual Report 1981
KBS Technical Reports 81-01 – 81-16
Summaries
Stockholm, April 1982

1982
TR 82-28
The KBS Annual Report 1982
KBS Technical Reports 82-01 – 82-27
Summaries
Stockholm, July 1983

1983
TR 83-77
The KBS Annual Report 1983
KBS Technical Reports 83-01 – 83-76
Summaries
Stockholm, June 1984

1984
TR 85-01
Annual Research and Development Report 1984
Including Summaries of Technical Reports Issued during 1984. (Technical Reports 84-01 – 84-19)
Stockholm, June 1985

1985
TR 85-20
Annual Research and Development Report 1985
Including Summaries of Technical Reports Issued during 1985. (Technical Reports 85-01 – 85-19)
Stockholm, May 1986

1986
TR 86-31
SKB Annual Report 1986
Including Summaries of Technical Reports Issued during 1986
Stockholm, May 1987

1987
TR 87-33
SKB Annual Report 1987
Including Summaries of Technical Reports Issued during 1987
Stockholm, May 1988

1988
TR 88-32
SKB Annual Report 1988
Including Summaries of Technical Reports Issued during 1988
Stockholm, May 1989

1989
TR 89-40
SKB Annual Report 1989
Including Summaries of Technical Reports Issued during 1989
Stockholm, May 1990

Technical Reports
List of SKB Technical Reports 1990

TR 90-01
FARF31 –
A far field radionuclide migration code for use with the PROPER package
Sven Norman[1], Nils Kjellbert[2]
[1]Starprog AB
[2]SKB AB
January 1990

TR 90-02
Source terms, isolation and radiological consequences of carbon-14 waste in the Swedish SFR repository
Rolf Hesböl, Ignasi Puigdomenech, Sverker Evans
Studsvik Nuclear
January 1990

TR 90-03
Uncertainties in repository performance from spatial variability of hydraulic conductivities –
Statistical estimation and stochastic simulation using PROPER
Lars Lovius[1], Sven Norman[1], Nils Kjellbert[2]
[1]Starprog AB
[2]SKB AB
February 1990

TR 90-04
Examination of the surface deposit on an irradiated PWR fuel specimen subjected to corrosion in deionized water
R. S. Forsyth, U-B. Eklund, O. Mattsson, D. Schrire
Studsvik Nuclear
March 1990

TR 90-05
Potential effects of bacteria on radionuclide transport from a Swedish high level nuclear waste repository
Karsten Pedersen
University of Gothenburg, Department of General and Marine Microbiology, Gothenburg
January 1990

TR 90-06
Transport of actinides and Tc through a bentonite backfill containing small quantities of iron, copper or minerals in inert atmosphere
Yngve Albinsson, Birgit Sätmark,
Ingemar Engkvist, W. Johansson
Department of Nuclear Chemistry,
Chalmers University of Technology, Gothenburg
April 1990

TR 90-07
Examination of reaction products on the surface of UO_2 fuel exposed to reactor coolant water during power operation
R. S. Forsyth, T. J. Jonsson, O. Mattsson
Studsvik Nuclear
March 1990

TR 90-08
Radiolytically induced oxidative dissolution of spent nuclear fuel
Lars Werme[1], Patrik Sellin[1], Roy Forsyth[2]
[1]Swedish Nuclear Fuel and waste Management Co (SKB)
[2]Studsvik Nuclear
May 1990

TR 90-09
Individual radiation doses from unit releases of long lived radionuclides
Ulla Bergström, Sture Nordlinder
Studsvik Nuclear
April 1990

TR 90-10
Outline of regional geology, mineralogy and geochemistry, Poços de Caldas, Minas Gerais, Brazil
H. D. Schorscher[1], M. E. Shea[2]
[1]University of Sao Paulo
[2]Battelle, Chicago
December 1990

TR 90-11
Mineralogy, petrology and geochemistry of the Poços de Caldas analogue study sites, Minas Gerais, Brazil
I: Osamu Utsumi uranium mine
N. Waber[1], H. D. Schorscher[2], A. B. MacKenzie[3], T. Peters[1]
[1]University of Bern
[2]University of Sao Paulo
[3]Scottish Universities Research & Reactor Centre (SURRC), Glasgow
December 1990

TR 90-12
Mineralogy, petrology and geochemistry of the Poços de Caldas analogue study sites, Minas Gerais, Brazil
II: Morro do Ferro
N. Waber
University of Bern
December 1990

TR 90-13
Isotopic geochemical characterisation of selected nepheline syenites and phonolites from the Poços de Caldas alkaline complex, Minas Gerais, Brazil
M. E. Shea
Battelle, Chicago
December 1990

TR 90-14
Geomorphological and hydrogeological features of the Poços de Caldas caldera, and the Osamu Utsumi mine and Morro do Ferro analogue study sites, Brazil
D. C. Holmes[1], A. E. Pitty[2], R. Noy[1]
[1]British Geological Survey, Keyworth
[2]INTERRA/ECL, Leicestershire, UK
December 1990

TR 90-15
Chemical and isotopic composition of groundwaters and their seasonal variability at the Osamu Utsumi and Morro do Ferro analogue study sites, Poços de Caldas, Brazil
D. K. Nordstrom[1], J. A. T. Smellie[2], M. Wolf[3]
[1]US Geological Survey, Menlo Park
[2]Conterra AB, Uppsala
[3]Gesellschaft für Strahlen- und Umweltforschung (GSF), Munich
December 1990

TR 90-16
Natural radionuclide and stable element studies of rock samples from the Osamu Utsumi mine and Morro do Ferro analogue study sites, Poços de Caldas, Brazil
A. B. MacKenzie[1], P. Linsalata[2], N. Miekeley[3], J. K. Osmond[4], D. B. Curtis[5]
[1]Scottish Universities Research & Reactor Centre (SURRC), Glasgow
[2]New York Medical Centre
[3]Catholic University of Rio de Janeiro (PUC)
[4]Florida State University
[5]Los Alamos National Laboratory
December 1990

TR 90-17
Natural series nuclide and rare earth element geochemistry of waters from the Osamu Utsumi mine and Morro do Ferro analogue study sites, Poços de Caldas, Brazil
N. Miekeley[1], O. Coutinho de Jesus[1], C-L Porto da Silveira[1], P. Linsalata[2], J. N. Andrews[3], J. K. Osmond[4]
[1]Catholic University of Rio de Janeiro (PUC)
[2]New York Medical Centre
[3]University of Bath
[4]Florida State University
December 1990

TR 90-18
Chemical and physical characterisation of suspended particles and colloids in waters from the Osamu Utsumi mine and Morro do Ferro analogue study sites, Poços de Caldas, Brazil
N. Miekeley[1], O. Coutinho de Jesus[1], C-L Porto da Silveira[1], C. Degueldre[2]
[1]Catholic University of Rio de Janeiro (PUC)
[2]PSI, Villingen, Switzerland
December 1990

TR 90-19
Microbiological analysis at the Osamu Utsumi mine and Morro do Ferro analogue study sites, Poços de Caldas, Brazil
J. West[1], A. Vialta[2], I. G. McKinley[3]
[1]British Geological Survey, Keyworth
[2]Uranio do Brasil, Poços de Caldas
[3]NAGRA, Baden, Switzerland
December 1990

TR 90-20
Testing of geochemical models in the Poços de Caldas analogue study
J. Bruno[1], J. E. Cross[2], J. Eikenberg[3], I. G. McKinley[4], D. Read[5], A. Sandino[1], P. Sellin[6]
[1]Royal Institute of Technology (KTH), Stockholm
[2]AERE, Harwell, UK
[3]PSI, Villingen, Switzerland
[4]NAGRA, Baden, Switzerland
[5]Atkins, ES, Epsom, UK
[6]Swedish Nuclear and Waste Management Co (SKB), Stockholm
December 1990

TR 90-21
Testing models of redox front migration and geochemistry at the Osamu Utsumi mine and Morro do Ferro analogue sites, Poços de Caldas, Brazil
J. Cross[1], A. Haworth[1], P. C. Lichtner[2], A. B. MacKenzi[3], L. Moreno[4], I. Neretnieks[4], D. K. Nordstrom[5], D. Read[6], L. Romero[4], S. M. Sharland[1], C. J. Tweed[1]
[1]AERE, Harwell, UK
[2]University of Bern
[3]Scottish Universities Research & Reactor Centre (SURRC), Glasgow
[4]Royal Institute of Technology (KTH), Stockholm
[5]US Geological Survey, Menlo Park
[6]Atkins ES, Epsom, UK
December 1990

TR 90-22
Near-field high temperature transport: Evidence from the genesis of the Osamu Utsumi uranium mine analogue site, Poços de Caldas, Brazil
L. M. Cathles[1], M. E. Shea[2]
[1]University of Cornell, New York
[2]Battelle, Chicago
December 1990

TR 90-23
Geochemical modelling of water-rock interactions at the Osamu Utsumi mine and Morro do Ferro analogue sites, Poços de Caldas, Brazil
D. K. Nordstrom[1], I. Puigdomenech[2], R. H. McNutt[3]
[1]US Geological Survey, Menlo Park
[2]Studsvik Nuclear, Sweden
[3]McMaster University, Ontario, Canada
December 1990